Journal of Volcanology and Geothermal Research 282 (2014) 43–59

Contents lists available at ScienceDirect

Journal of Volcanology and Geothermal Research

journal homepage: www.elsevier.com/locate/jvolgeores

Evolution of clay mineral assemblages in the Tinguiririca geothermal field, Andean Cordillera of central Chile: an XRD and HRTEM-AEM study

M. Vázquez [a,*], F. Nieto [b], D. Morata [a], B. Droguett [a,c,1], F.J. Carrillo-Rosua [b], S. Morales [b]

[a] Department of Geology and Andean Geothermal Center of Excellence (CEGA), Facultad de Ciencias Físicas y Matemáticas, Universidad de Chile, Plaza Ercilla 803, Santiago, Chile
[b] Departamento de Mineralogía y Petrología and Instituto Andaluz de Ciencias de la Tierra, Universidad de Granada-CSIC, Avenida Fuentenueva, 18002 Granada, Spain
[c] Energía Andina S.A, Cerro El Plomo 5630, Santiago, Chile

ARTICLE INFO

Article history:
Received 9 December 2013
Accepted 26 May 2014
Available online 21 June 2014

Keywords:
Geothermal alteration
Clay minerals
Reaction progress
XRD
HRTEM-AEM
Andean Cordillera
Chile

ABSTRACT

HRTEM textural evidence shows that clay minerals in the Tinguiririca geothermal field (Andean Cordillera, central Chile) are the result of direct alteration of former volcanic glass and minerals by hydrothermal fluids at similar temperatures to the present day. They show the classical pattern of diagenetic transformation from smectite at the top to illite at the bottom, with the progressive formation of corrensite and chlorite. The high fluid/rock ratio, disposability of necessary cations and absence of previous detrital phyllosilicates allow the consideration of this area as a natural laboratory to establish the extreme ideal conditions for very low-T reactions. Transformations from smectite to R1 illite–smectite (I–S) and from these to R3 mixed-layers occur respectively at 80–120 °C and 125–180 °C. In spite of ideal genetic conditions, the new-formed minerals show all the defective character and lack of textural and chemical equilibrium previously described in the literature for diagenetic and hydrothermal low-temperature assemblages. Chemistry of smectite–illite phases evolves basically through a diminution of the pyrophyllitic component toward a theoretical muscovite ($Si^{4+} + \square \rightarrow Al^{3+} + K^{+}$). However, a second chemical vector ($Si^{4+} + Mg^{2+} \rightarrow Al^{3+} + Al^{3+}$), that is, decreasing of the tschermack component, also contributes to the evolution toward the less Si-more Al rich muscovite in relation to the original smectite. Residual Mg (and Fe) from the latter reaction is consumed in the genesis of chloritic phases. Nevertheless, as a consequence of the lack of chemical equilibrium (probably because of the short time-scale of the geothermal alteration processes), the composition of clay minerals is highly heterogeneous at the level of a single sample. Consequently, the respective fields of smectite, R1 I–S and R3 I–S overlap each other, making the distinction among these three phases impossible based exclusively on chemical data.

1. Introduction

A progressive series of clay mineral reactions occurs during diagenesis; these reactions increase the sediment density and reduce pore-space as new, bedding-parallel authigenic phyllosilicates invade and fill voids (Merriman and Peacor, 1999). Most clay minerals progressively change from random-oriented to a more or less oriented fabric when the conditions of low-temperature metamorphism are attained. The physical, mineralogical and chemical modifications exhibited by phyllosilicates during diagenesis are widely applied in petroleum exploration, allowing the identification of the necessary conditions for the transition from dry-gas phase to unproductive rocks, which occurs during the evolution from deep diagenesis to anchizone.

During low-temperature processes, thermodynamic equilibrium is not attained by the paragenesis of clay minerals (Merriman et al., 1995; Árkai et al., 1996; Warr and Nieto, 1998; Árkai et al., 2000; Abad et al., 2001, 2003a, 2003b). The mineralogical transformations are controlled, in addition to temperature and pressure, by other additional factors such as the original material and the chemical composition, time, fluid/rock ratio and tectonic stress. Consequently, the crystal–chemical parameters of phylloslilicates cannot be used for geothermometric determinations. The clay mineral reactions are governed by the Ostwald Step Rule (Morse and Casey, 1988), which states that the clay mineral paragenesis evolves through the formation of successive metastable phyllosilicates that progress toward the state of stable chemical and textural equilibrium (eg. Nieto et al., 1996). This is reached during greenschist-facies (Abad et al., 2006). However, the characteristics of clay minerals are qualitative indicators of the reaction progress, in other words, the stage which phyllosilicates have reached through a series of metastable mineral reactions (Merriman and Peacor, 1999).

A plethora of researchers have studied clay minerals in low-temperature processes. Nevertheless, no agreement exists about the temperature for the various mineral changes or the mineral genesis mechanism. Smectite illitization and the formation of chlorite are the processes most often referred to in the literature. Smectite illitization

* Corresponding author. Tel.: +56 2 29784539; fax: +56 2 26963050.
E-mail address: mvazquez@ing.uchile.cl (M. Vázquez).
[1] Current address: Amawta consultores. Almirante Pastene 185, Santiago, Chile.

http://dx.doi.org/10.1016/j.jvolgeores.2014.05.022
0377-0273/

onset is marked by the disappearance of smectite or R0 illite–smectite mixed-layers (hereafter, I–S) and the formation of R1 I–S. This occurs at temperatures from 75 to 120 °C (Hoffman and Hower, 1979; Srodon and Eberl, 1984; Schegg and Leu, 1996; Uysal et al., 2000; Abid et al., 2004). The transition from R1 to R3-ordered I–S occurs up to 175 °C (Hoffman and Hower, 1979; Weaver, 1989; Lindgreen, 1991; Pollastro, 1993; Abid et al., 2004). However, the temperature of this mineralogical change could be higher and depends on the characteristics of the original materials (eg. Arostegui et al., 2006). Additionally, illitization can be inhibited in sediments with low K contents and low porosity and/or in sediments with high Mg and Ca contents. On the other hand, the temperature of chlorite formation is between 100 and 270 °C, broadly coinciding with the development of I–S.

Hydrothermal systems offer a simpler scenario for the study of low-T processes under a more constrained set of parameters. The presence of a sufficient hot fluid phase in these hydrothermal systems compared with restricted and limited water availability in diagenetic transformations during burial would imply a higher fluid/rock ratio that could guarantee a more rapid and complete evolution and, in part, liberates the system from the influence of the original material. Clay minerals are widespread alteration products in most active and fossil geothermal systems, being excellent tracers of their hydrothermal history (e.g. Mas et al., 2003, 2006 and references therein). Many studies have considered both the sequential distribution from smectites to non-expandable di- or trioctahedral phyllosilicates and the chemical variations of the non-expandable clay phases (e.g. chlorite and/or illite) as a function of past or present thermal conditions (e.g. Cathelineau and Nieva, 1985; Ji and Browne, 2000). However, properties of clay minerals are not only affected by temperature but also by rock and fluid chemistry, time, fluid/rock ratio, the nature of the precursor material or mechanism of crystal growth (e.g. Essene and Peacor, 1995; Lopez-Munguira et al., 2002). These factors affect the structure (coherent domain size in the c-direction, polytypism, mixed-layering), composition (cation site occupancy) and texture (particle size, morphology). Consequently, the conditions at which these minerals crystallized in the active and fossil geothermal fields are more properly approached by an integrated study of all the crystal parameters of clay minerals at the field scale.

The Salton Sea geothermal field in southeastern California has long been of interest to geologists as an area of hydrothermal metamorphism of detrital sediments, from diagenesis to greenschist facies, with a continuous progression of minerals as a function of depth (Muffler and White, 1969). White mica, chlorite and biotite were found to change gradually from the initial fine-grained materials to coarser-grained, more mature crystals, suggesting continued growth of crystals with burial, as consistent with the concept of burial metamorphism. Yau et al. (1987a, b, 1988) utilized transmission, analytical and scanning electron microscopy (TEM, AEM, SEM) to characterize the minerals and the processes of transformation. They described three phyllosilicate zones: (1) illite–muscovite (115–220 °C), (2) chlorite (220–310 °C), (3) biotite (>310 °C). Giorgetti et al. (2000) showed that in the shallowest parts of this geothermal field the detrital kaolinite and muscovite reacted to form interstratified illite–smectite (I–S), which in turn was replaced by illite. The textures and microstructures observed indicate that the mineral progression involves dissolution of original phases, mass transport through interconnecting pore space, and direct crystallization of phyllosilicates from solution (eg. Yau et al., 1988; Giorgetti et al., 2000, 2003). Phyllosilicate changes with depth were not time-dependent, because they formed simultaneously at all depths as a result of a single hydrothermal event in an open system (Giorgetti et al., 2003).

The continuous slim hole core (815 m depth) drilled in the Tinguiririca geothermal field in the Andean Cordillera of central Chile by the company Energia Andina (EASA) offers an excellent case study of clay mineral evolution in an active geothermal system. Various kinds of mixed layers, both in the smectite–illite system and in the smectite–chlorite system are present, which can be correlated with the present day temperatures directly measured in the borehole and contrasted if the observed secondary mineralogy is consistent with *in situ* measured temperature.

The aim of this study is to determine the textural, mineral and chemical characteristics at the lattice level of the clay minerals in relation to depth in the active Tinguiririca geothermal system (Andean Cordillera of central Chile). The possibility of continuous sampling along the drill core will provide a thermal reference for the usually employed reaction progress parameters, as mineral paragenesis, type of mixed-layer and chlorite thermometry.

2. Geological setting

Geothermal resources in the Andean Cordillera of Chile are spatially associated with active volcanism, which is primarily controlled by the convergence of the Nazca and South America Plates. This geological setting constrains the Chilean Andean volcanic arc as one of the largest but not yet developed geothermal areas of the world. Consequently, two main volcanic zones can be distinguished within the Chilean Andes: the Northern Volcanic Zone (17°S–28°S) and the Central–Southern Volcanic Zone (33°S–46°S) parallel to the coast.

Few studies regarding the mineralogy involved in low temperature alterations have thus far been developed in Chile (e.g. Droguett et al., 2012), with most of the published papers being focused on fossil geothermal systems in the central Andean Cordillera (Vergara et al., 1993; Aguirre et al., 2000; Fuentes et al., 2004). The Tinguiririca Geothermal field, located only 150 km southwest of Santiago, developed on the Pleistocene–Holocene volcanic rocks of the Tinguiririca volcano (Fig. 1). The oldest geological units outcropping in the area belong to the Jurassic volcanic and volcaniclastic Rio Damas formation and the Jurassic Baños del Flaco limestone sequences. Cretaceous to Eocene–Miocene volcanic and volcaniclastic sequences overlie these sequences. All these units were folded and thrusted according to the major extensional and compressional deformation events (Clavero et al., 2011). Miocene subvolcanic stocks intrude Oligo-Miocene volcanic sequences. These deformed Meso-cenozoic units are unconformably overlain by the Lower to Upper Pleistocene Tinguiririca Volcanic Complex, mostly composed of subhorizontal calc-alkaline porphyritic basaltic to andesitic lava flows with minor pyroclastic levels. Based on K/Ar whole rock dating, Arcos et al (1988) suggested two main volcanic sequences during the building of the Tinguiririca Volcanic Complex. The oldest units were developed during the Lower Pleistocene (1.101 ± 0.068 to 0.922 ± 0.048 Ma), and the youngest during the Upper Pleistocene (0.297 ± 0.028 to 0.170 ± 0.030 Ma). Minor Holocene post-glacial volcanic cones were also identified in this volcanic complex. Calcic plagioclase, clino and orthopyroxene and minor olivine and magnetite are the main phenocrysts within an intersectal to hialopilitic groundmass. Three main volcanic cones (Tinguiririca, Fray Carlos and Montserrat) comprise this volcanic complex (Arcos et al., 1988). The NNE alignment of these volcanic cones is coincident with the main NNE fault system observed in the area, suggesting a strong structural control on the magmatic and also fluid paths in this section of the Andean Cordillera (Clavero et al., 2011).

Geothermal manifestations in the Tinguiririca volcanic field comprise steam vents, bubbling mud pools and flowing hot springs associated with steam-heated, acid sulfate and near neutral pH bicarbonate waters (Clavero et al., 2011). These surficial geothermal manifestations occur to the west and southwest of the Tinguiririca volcano, between 2700 and 3300 m (Fig. 1). Water and gas geochemistry together with He isotope ratios suggests equilibrium temperatures in between 230° to 300 °C having He a clear magmatic source, possibly related with basaltic systems (Clavero et al., 2011). A first explorative 815 m depth continuous core (Pte-1 borehole) was drilled by Energia Andina on the southwestern flank of the volcanic complex (Fig. 1). The well lithology, dominated by Pliocene basaltic andesite lava flows and minor intercalated volcaniclastic layers, is summarized in Fig. 2. According to geological, geochemical and geophysical data, the geothermal reservoir could

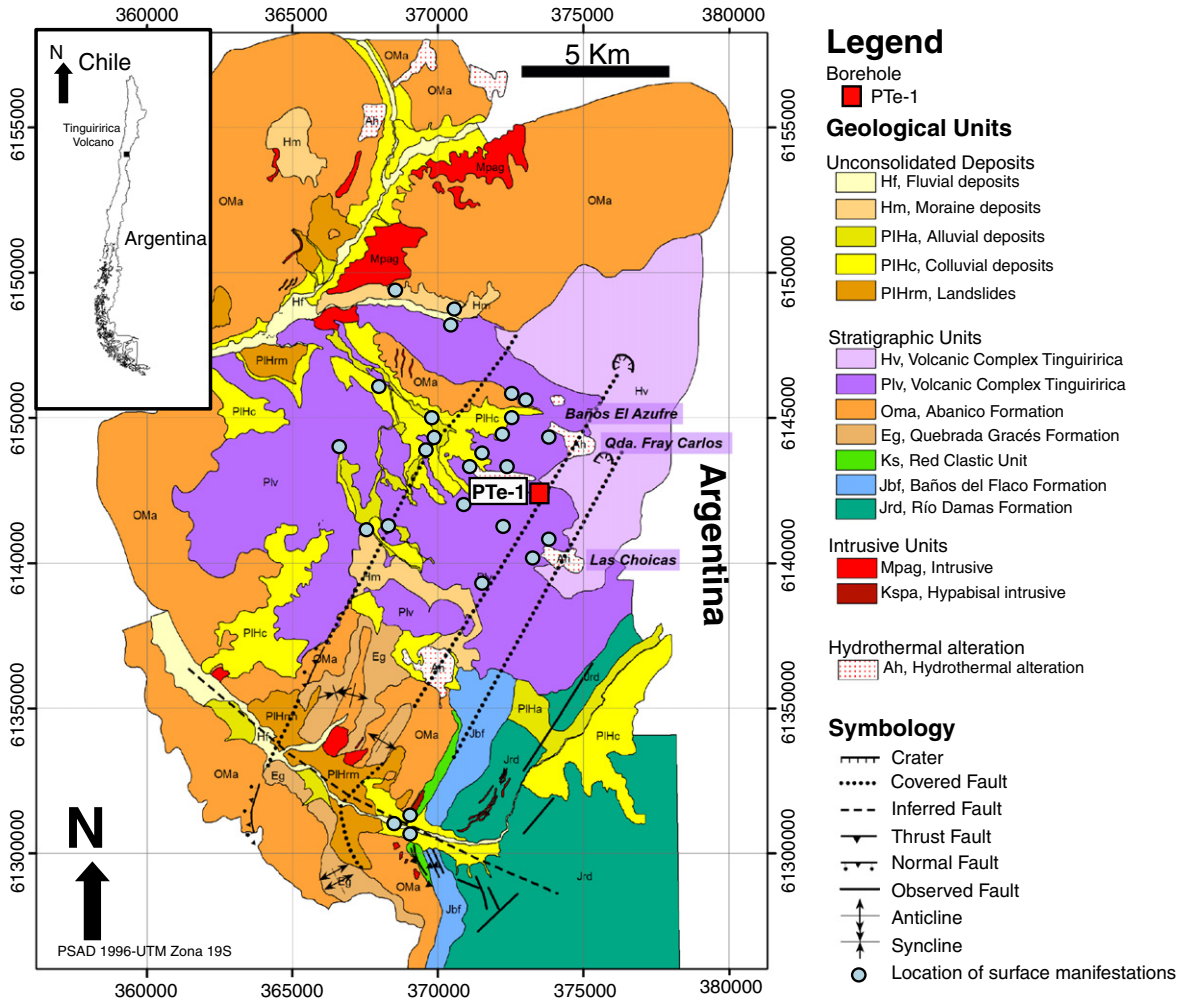

Fig. 1. Geological map of Tinguiririca geothermal field simplified from Clavero et al. (2011).

be hosted in the Oligo-Miocene volcanic and volcaniclastic units (not drilled in Pte-1 borehole) as well as in the lower part of the Pliocene volcanic sequences (Clavero et al., 2011).

Droguett et al. (2012) determined the geothermal alteration mineralogy of the Tinguiririca geothermal field (Fig. 2), using petrographic techniques, XRD and SEM. Samples were collected along the Pte-1 borehole, where the temperature was directly measured along the 813 m drill core. In the shallowest parts of the borehole (0–410 m), variaties of silica (mostly chalcedony according to petrographic characteristics) and iddingsite are present as index phases and hydrated Ca-Al silicates like wairakite (XRD and optical identification), prehnite and epidote together with quartz appear in the deepest ones (600–813 m) developing propylitic alteration consistent with almost neutral pH fluid conditions. The alteration minerals appear filling open spaces (voids and fractures), in the volcanic groundmass and as pseudomorphous of primary (mostly plagioclase) phases (Fig. 3).

3. Material and methods

Eighteen samples were selected along the Tinguiririca borehole for clay mineral characterization using X-ray diffraction (XRD) and, from them, four samples were chosen for high-resolution and analytical transmission electron microscopy (HRTEM-AEM).

The depths of the samples studied along the borehole are shown in Fig. 2. The rocks of the drill core show a compact texture and small grain size, showing intense clay alteration inside the vitreous matrix. The color of the samples along the borehole is generally dark gray, with greenish tones at some depth of the upper part of the borehole. The vein fillings of calcite and various silica phases are common along the borehole.

Fig. 2 shows the alteration mineralogy determined by Droguett et al. (2012) along the hole and the directly measured temperature during drilling. In the following, the samples will be named according to their depth in meters.

The samples were crushed with a laboratory jaw-crusher. The <2 μm fraction was separated by centrifuge, and then smeared onto glass slides. In some cases, it was necessary to remove the carbonates. A solution of 0.2 N HCl was added to the suspension of crushed rocks and agitated continuously for 10 min. We have used the recommendations by Moore and Reynolds (1997) in order to identify the different kind and proportion of the mixed layer minerals.

The XRD data were obtained with three different difractometers (1) Philips PW 12050/25 powder diffractometer with CuKα radiation at Mineralogic & Petrologic Solutions Ltd (New Zealand); (2) Philips PW 1710 powder diffractometer with CuKα radiation, graphite monochromator and automatic divergence slit at the Departament of Mineralogy and Petrology of the Universidad de Granada and (3) Bruker D8 Advanced diffractometer with Cu-Kα radiation with a Bragg–Brentano geometry at the Department of Physics in the Faculty of Sciences and Engineering of the Universidad de Chile. Clay minerals in this fraction were identified according to the position of the basal reflections on XRD patterns of air-dried, ethylene-glycolated (EGC), and heated (300 °C for 2 h). Illite–smectite (I–S) and chlorite–smectite (C–S) mixed-layer clay minerals were identified and the respective

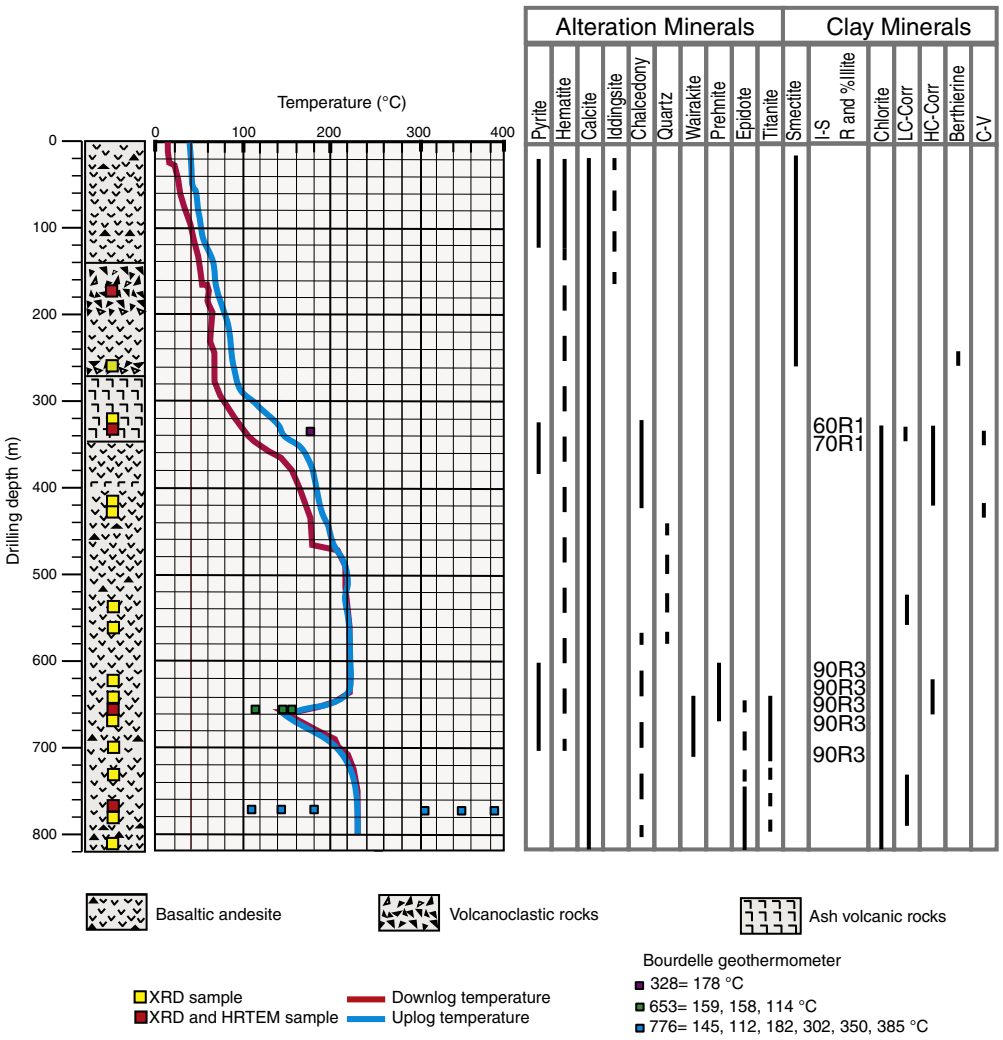

Fig. 2. Lithology and distribution of secondary minerals determined by Droguett et al. (2012) in PTe-1. Clay minerals distribution is also plotted according to their sampling depth. The values of temperature calculated by Bourdelle et al. (2013) geothermometer, using chlorite composition presented on Table 2, are shown. I–S: illite–smectite minerals; R = I–S Ordering; HC-Corr: High-charge corrensite; LC-Corr: Low-charge corrensite; C–V: chlorite–vermiculite mixed layers.

proportions of illite and chlorite components determined according to Moore and Reynolds (1997) criteria. Heat treatments were useful for the identification of vermiculite layers in the chlorite mixed layered phases.

The HRTEM studies were performed using two high resolution microscopes at the Universidad de Granada (Spain): (1) a Philips CM-20 scanning transmission electron microscope (STEM), working at 200 kV with a point to point resolution of 2.7 Å in the TEM mode. (2) A Titan with XFEG emission gun, spherical aberration corrector and HAADF detector, working at 300 kV, with a resolution of 0.8 Å in the TEM mode and 2 Å in the STEM mode. Copper rings were attached to representative selected areas of the matrix of the thin-sections. These areas were detached through gentle heating. Samples were further thinned with a Gatan dual ion mill using an acceleration voltage of 6 kV during three stages: (1) incidence angle of 15° and probe current of 1 nA; (2) incidence angle of 15° and probe current of 0.6 nA; (3) incidence angle of 12° and probe current of 0.4 nA. Chemical analyses of clay minerals were made in STEM mode with an EDAX microanalisis system. A 200*1000 Å scanning area with the long axis oriented parallel to phyllosilicate packets was used for each analysis using a 50 Å beam diameter. Chemical compositions were obtained from two kinds of samples: from the copper rings, previously described, to correlate chemical compositions with high resolution images and from individual particles from powdered portions, dispersed onto C-coated Cu grids. The data thus obtained are complementary to those taken from ion-milled samples as their orientation allows the use of a larger scanning window for analysis, which provides better reproducibility of data and less loss of alkalis. Counting times of 100 s were used except for Na and K, which were analyzed using 30 s counting times (Nieto et al., 1996). Albite, olivine, biotite, spessartine, muscovite, chlorite and titanite were used to obtain K factors for transformation, according to Cliff and Lorimer (1975).

4. Results

4.1. X-ray diffraction

The mineralogy of the clay fraction determined by XRD and corresponding treatments is showed in Fig. 2. Mixed layers, such as illite–smectite (I–S), corrensite (Corr) and chlorite–vermiculite (C–V) have been identified in several segments of the borehole from Tinguiririca geothermal fields.

I–S mixed layers has been determined comparing the air-dried and ethylene glycol treated specimens (Fig. 4a). Illite proportion of I–S was determined by the position of the reflection near 16° to 17° 2θ and the ordering type by the position of the reflection from 5° to 8.5° 2θ for ethylene glycol solvated preparations (Fig. 4a).

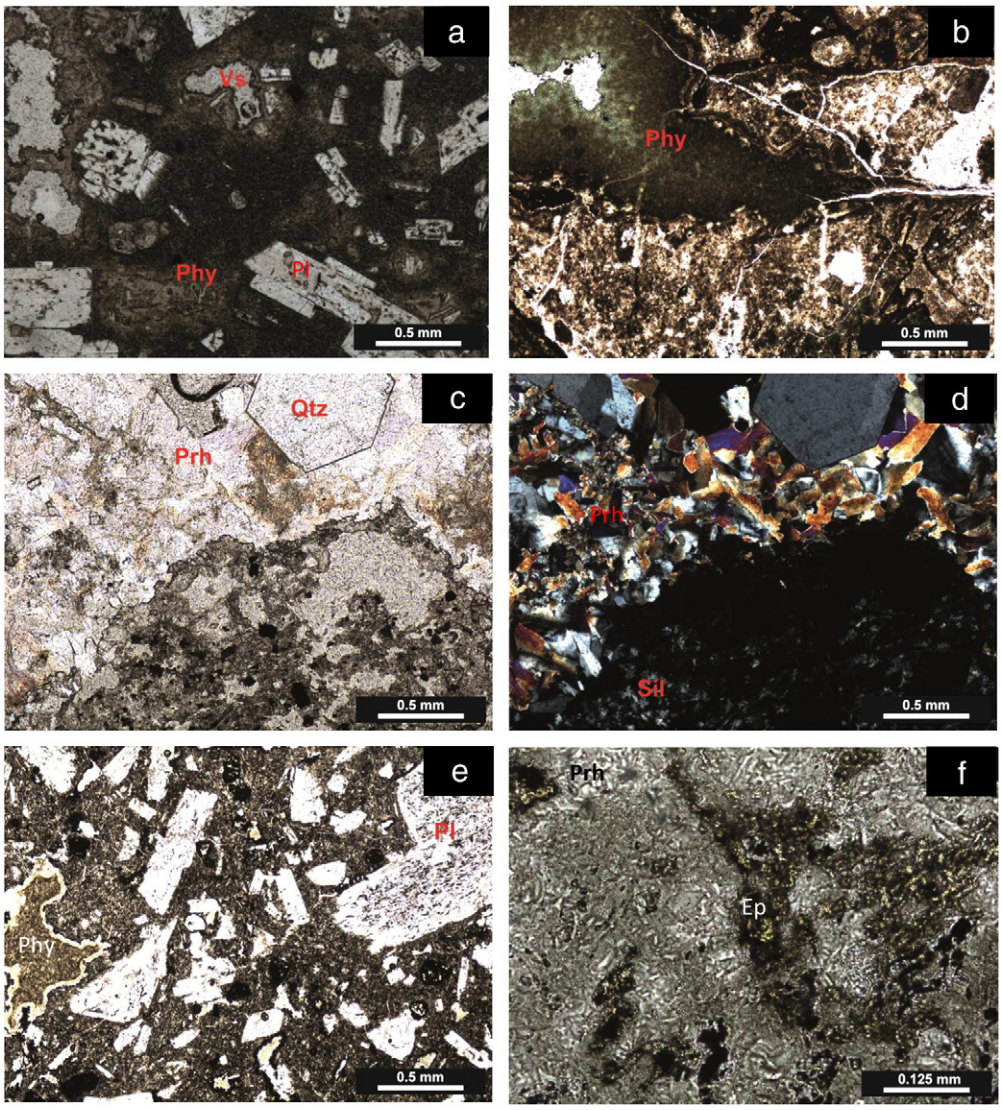

Fig. 3. Optical photomicrograph of the samples of Pte-1 borehole. (a) Porphyroblasts of plagioclase (Pl) partially replaced by phyllosilicates (Phy) and vesicle (Vs) are present in 158 sample. (b) Phyllosilicates filling voids in 262 sample. (c) Prehenite (Prh) and quartz, adjacent to silica phase in 595 sample. (d) Crossed-nicols image of (c). (e) Phyllosilicates filling pores and as main constituent of the matrix in 699 sample. (f) Epidote (Ep) and Prehenite (Prh) are present as secondary minerals in 786 sample.

Chloritic-like phases with a more intense 14 Å peak than the 7 Å one have been observed in air-dried samples from several segments of the borehole (e.g. Fig. 4b). We have compared the air-dried and 300 °C heated samples for determining the kinds of phyllosilicate layers present. Fig. 4 shows peaks on the sloping background at ~28 Å in the air-dried sample, which is also compatible with the presence of corrensite. Low-charge corrensite appears in some samples, detected by the 28 Å peak which expands to 31 Å after EG-solvation (Fig. 4a and b). Heat treatment at 300 °C for 2 h resulted in one plateau with spacings ranging from 7 to 8 Å, respectively (Fig. 4b). This broad plateau is interpreted as a convolution of 002 (~7 Å) of chlorite and 003 (~8 Å) of collapsed corrensite. High-charge corrensite has been detected by the presence of the peak at 28 Å, which is unaffected by EG-solvation. Heat treatments also reveal the presence of a chlorite–vermiculite mixed layer in some samples. The presence of vermiculite layers generates significant changes in the intensity and basal spacing of chlorite. In this way, 001 of chlorite is 14.22 Å in air-dried samples, while in the heated samples appear the characteristic peak of chlorite at 14.13 Å. Both kinds of corrensite coexist in some samples (e.g. Fig. 4a). The peak deconvolution at ~29 Å in EG samples (not shown) confirms the presence of two peaks, one at 31 Å and the other at 28 Å, corresponding respectively to low and high charge corrensite.

The distribution of the clay minerals along the borehole shows a zonation according to the depth (Fig. 2). Smectite is present at the shallow parts of the borehole together with berthierine, identified by their peaks (001) at 7.07 Å and (002) at 3.54 Å. Below, I–S mixed layers appear instead of smectite. Interstratified clays show progressive illitization with increasing depth, from 60% of Illite layers with R1 order at 325 m to more than 90% of Illite layers with R3 order from 408 m. From this depth, I–S R3 mixed layers with minor content of expandable layers (<10% of smectite) have been identified. Chlorite and high-charge corrensite appear together with I–S mixed layers. C–V mixed layers only were identified at 408 m. Low-charge corrensite was identified at the bottom of the borehole. At this depth chlorite is present in addition to low-charge corrensite.

4.2. Transmission electron microscopy

Selected samples representing each of the phyllosilicate mineral zones found by XRD (Fig. 2) were examined by TEM in order to characterize the mineralogy, textural relationships and chemical composition of the clay minerals along the borehole.

Typical TEM textures from each depth are shown in Fig. 5. At low magnification, TEM images show similar textures in the analyzed

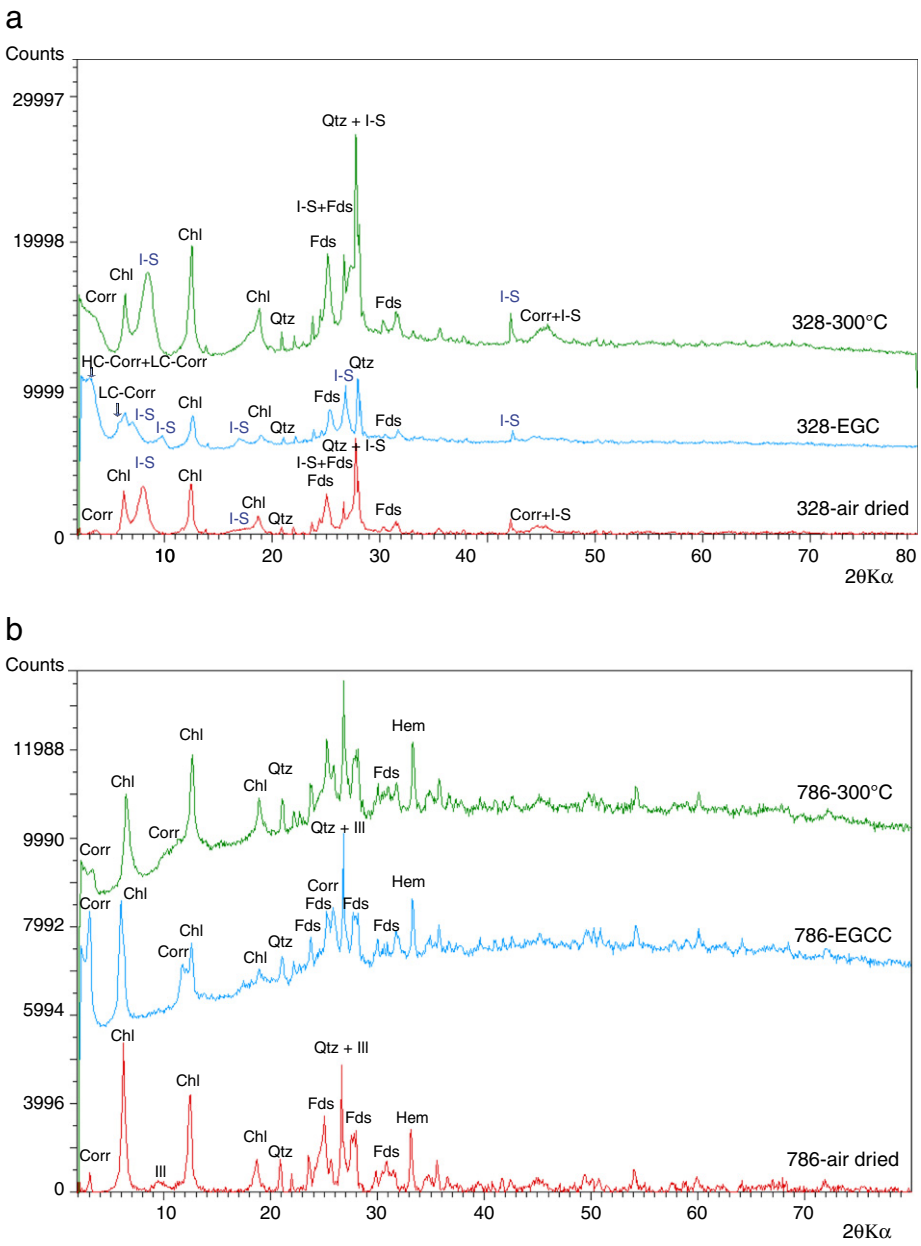

Fig. 4. XRD diagrams of the mixed layered clay minerals. (a) Illite–smectite (I–S) with 70% of illite and R1 ordering and low-charge corrensite in 328 sample, air-dried, EG solvated and heated to 300 °C. (c) Low-charge corrensite in 786 sample, air dried, EG solvated and heated to 300 °C.

samples. Clay minerals replace plagioclase and volcanic glass and show curved, lens-shaped morphology and no preferred orientation. Smectite appears filling pores inside of plagioclase crystals at 158 m of depth (Fig. 5a). Smectite shows a ribbon-like morphology (Güven and Grim, 1972; Grim and Güven, 1978). I–S mixed layers can be recognized at the HAADF image of sample 328 showing a similar texture to smectite (Fig. 5b), with curved and lens-shaped morphology and no preferred orientation. Volcanic glass has been recognized in sample 328 by its composition and completely amorphous character (absence of diffraction spots in SAED). It is apparent from Fig. 5c the genetic relationship between glass and the process of dissolution–precipitation which occurred during the crystallization of I–S mixed layers. Low-charge corrensite appears filling irregular cavities of plagioclase, providing direct evidence for neocrystallization from hydrothermal fluids (Fig. 5d).

4.2.1. Sample 158

Smectite packets exhibit a lens-shaped morphology in TEM images, with no preferred orientation (Fig. 6a). The smectite is characterized by discontinuous, wavy fringes, with d-spacings of 10 Å. The smectite layers are curved with their orientation changing along the packet and the number of parallel layers is very small, frequently lower than four. The various sub-packets, considering these as areas constituting a coherent crystalline domain, show an anastomosing relationship to each other, with frequent layer terminations at low-angle contacts with the neighbor sub-packet. In Fig. 6b, partial two-dimensional resolution allows measuring 4.5 Å as the crystalline parameter along the layers. This distance corresponds to half b parameter of the phyllosilicates (reflection 020). In those areas in which the two-dimensional resolution persists at less for three lattice fringes, local coherence between the parallel layers may be recognized, with the fringes perpendicular to the smectite layers and showing continuity from layer to layer. In adjacent layers also an angle of ~60° may be measured between the two families of fringes, which, according to Dong and Peacor (1996) correspond to the (112) reflection. This situation is similar to the case described by Dong and Peacor (1996) for Gulf Coast smectites and coherent with the model proposed by Guthrie and Reynolds (1998).

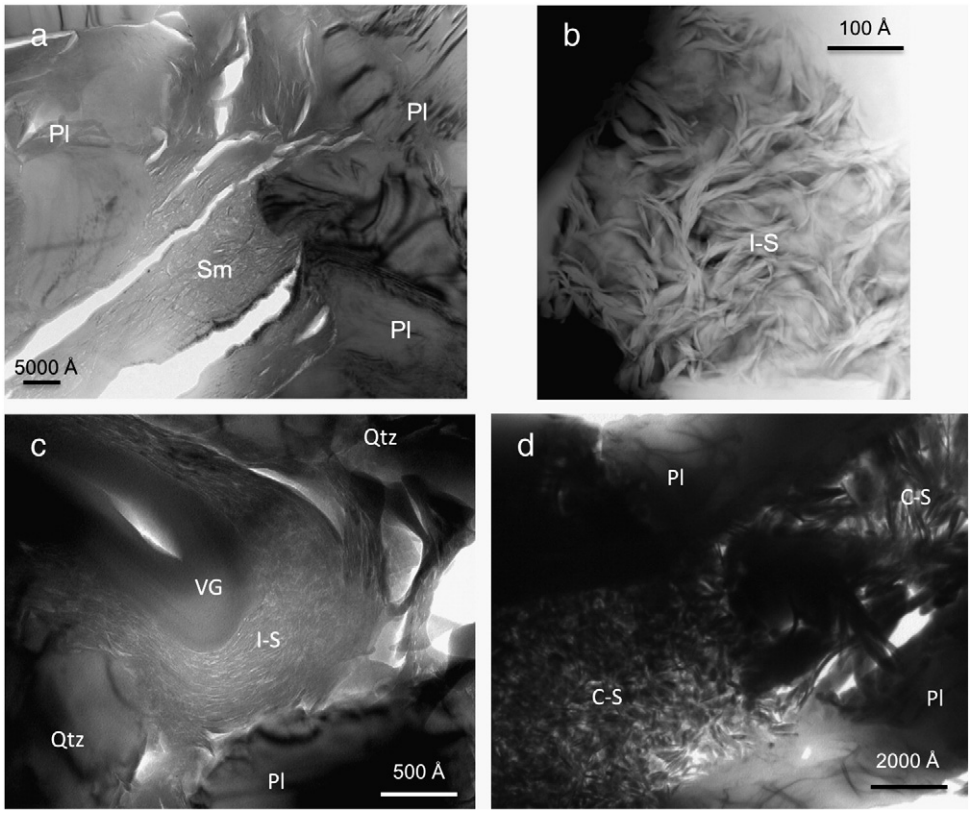

Fig. 5. Textural images of clay minerals. (a) Smectite (Sm) filling voids of plagioclase (Pl) in 158 sample. (b) HAADF image of I–S mixed layers showing curved and lens-shaped morphology and no preferred orientation in 328 sample. (c) Volcanic glass (VG) transformed to I–S mixed layers, quartz (Qtz) and plagioclase in 328 sample. (d) Low-charge corrensite filling irregular cavities of plagioclase in 776 sample.

Minor packets showing 7 Å spacing are visible in some areas. Peaks corresponding to such spacing are absent in the XRD diagram, probably due to their rarity in the sample; however berthierine was identified by XRD in sample 262. Therefore, we tentatively interpret those fringes as corresponding to berthierine.

4.2.2. Sample 328

Fig. 7 shows typical lattice fringe images of this sample. Illite–smectite mixed layers show defective texture similar to smectite from sample 158. In this way, the I–S displays curved small packets (25 nm thick), similar to the smectite (Fig. 7a). Also an anastomosing relationship between the various sub-packets is evident. Consequently in most of the cases the crystalline domain size is formed by no more than 4–10 layers.

In some areas, fringes show alternating dark and light contrast, typical of I–S mixed-layers (Fig. 7b). Guthrie and Veblen (1989a, 1989b, 1990) and Veblen et al. (1990) described that in normal routine conditions smectitic and illitic layers cannot be distinguished, but some particular conditions in the TEM can allow their differentiation. Therefore, we can expect packets formed by 10 Å layers as those shown in Fig. 7a. Differences of contrast will be visible only in some particular areas (Fig. 7b), which fulfil the particular conditions necessary to produce differences of contrast or spacing. Fringes with spacing of 22, 32 or 35 Å periodicity, characteristic of the sum of one or two illite and one smectite layer spacing in R = 1 I–S (Kim et al., 1995; Dong et al., 1997) can also be recognized. Non-001 reflections are ill-defined, nonperiodic and diffuse parallel to c* (Fig. 7a, inset), implying that stacking is generally random. Such SAED patterns have commonly been found to be diagnostic of $1M_d$ polytypism.

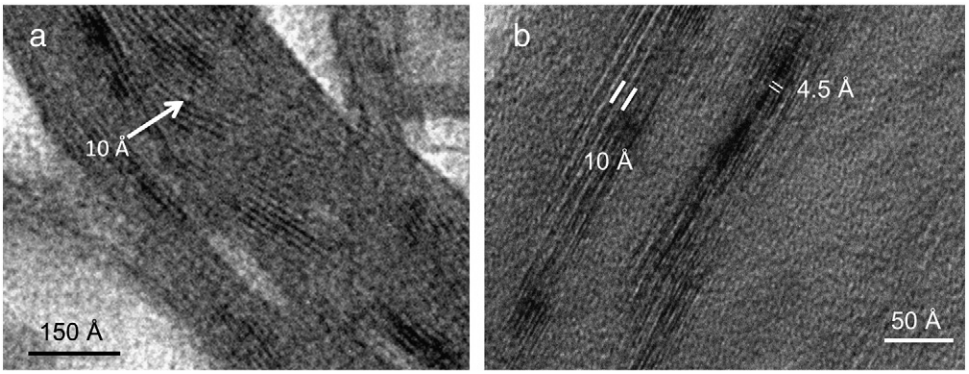

Fig. 6. Smectite in 158 sample. (a) Smectite with lens-shaped morphology. (b) Discontinuous and wavy fringes of smectite with two families of d-spacings at 10 and 4.5 Å.

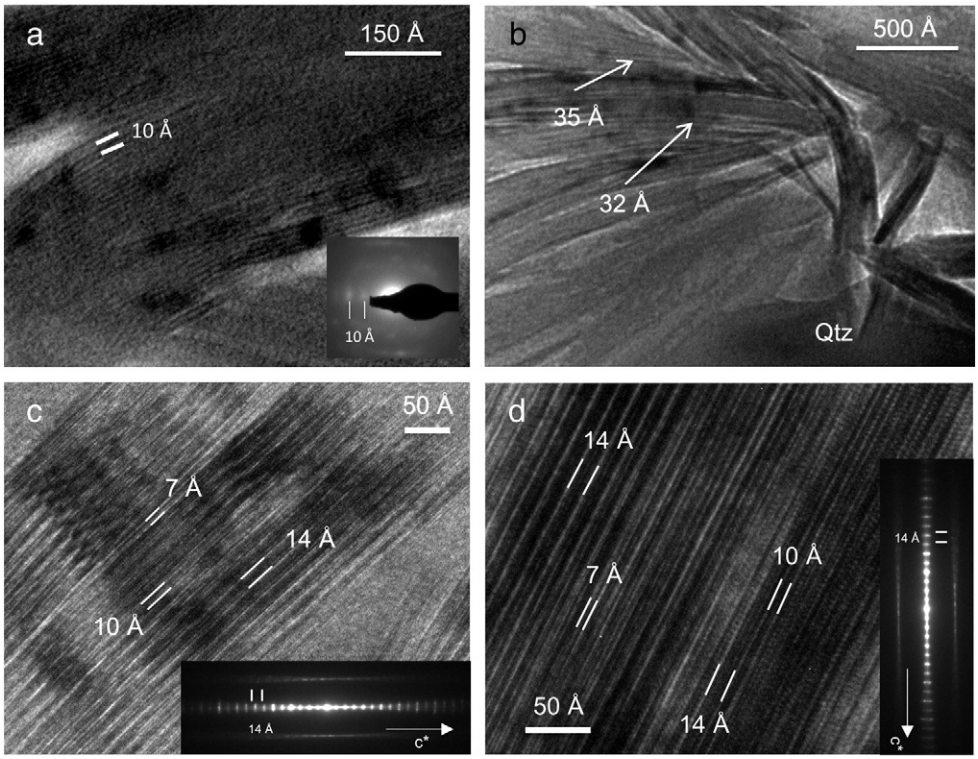

Fig. 7. Clays mixed layers in 328 sample. (a) Illite–smectite (I–S) mixed layers show curved small packets. Non-001 reflections are ill-defined, non-periodic and diffuse parallel to c*, implying that stacking is generally random. Such SAED patterns are typical of 1Md polytypism. (b) The fringes have spacing (22 to 35 Å periodicity) characteristic of the sum of illite- and smectite-like layer spacings in (R = 1) I–S. (c) and (d) Chlorite intergrowth and/or interstratified with 10 Å and 7 Å layers.

Chlorite is usually intergrown and/or interstratified with 10 Å and 7 Å layers (Fig. 7c and d). In some cases small packets (20 nm thick) of pure chlorite may be recognized. The presence of 10 Å layers is coherent with the XRD results, which have shown chlorite and corrensite in the samples of this part of the borehole. Intermixing and interlayering of berthierine have been frequently described in low-temperature chlorite and it is a consequence of the metastable character of the former (Abad-Ortega and Nieto, 1995 and references therein). SAED always shows a disordered polytype for chlorite (Fig. 7c and d, inset), which, at least in part, may be a consequence of the previously described interstratified layers.

4.2.3. Sample 653

Small packets of illite have been observed in sample 653, with a typical packet size of 30 nm thick (Fig. 8a and b). Curvature and the general high defective character of previously described samples are absent (Fig. 8a and b). Straight boundaries and defect-free lattice fringes are a renowned characteristic. The size and characteristics are similar to those typical of the low-anchizone in diagenetic evolution (Merriman and Peacor, 1999). High magnification images show the presence of lattice fringes with spacing of 10 and 20 Å. Differences in contrast or spacing, indicative of minor smectite layer presence have not been recognized. Nevertheless, as stated by Guthrie and Veblen (1989a), this fact is not conclusive about the complete absence of smectite layers and, according to the XRD, illite–smectite (I–S) mixed-layers with R3 order and a content of illite layers higher than 90% are the dominant illitic phase. We assume, therefore, that minor smectite layers should be present but they are not distinguishable from the illitic layers.

Two kinds of SAED patterns for the illite packets have been recognized: (1) SAED patterns with well defined (001l) reflections at 10 Å, with diffuseness normal and parallel to c*, implying that stacking is generally random and therefore corresponding to $1M_d$ polytypism (Fig. 8a); and (2) SAED patterns with non-001 reflections showing a well defined periodicity at 20 Å, indicating that they correspond to a well-ordered 2-layer polytype (Fig. 8b), probably $2M_1$. The 001 row has additional weak reflections producing 20 Å periodicity due to dynamical effects. No relationship between size of packets and polytype has been found.

Usually, at least two different orientations are recognized in the SAED. One includes c* and b* (or equivalent direction) and the other c* and a* (or equivalent direction). Normally a SAED is obtained from an area that includes various packets. These packets are differently oriented in relation to the c* direction, but also in the a*–b* plane.

Chlorite (Fig. 8c) is present in small packets (20 nm). They are often free of 10 Å layers. Their polytype always appears disordered (Fig. 8c inset).

4.2.4. Sample 776

The major phyllosilicate in the sample is chlorite, which presents variable interstratification with 10 Å layers (Fig. 9). In some cases packets showing 24 Å layers can be recognized (Fig. 9a). They represent the ordered sum of one chlorite layer (14 Å) and one contracted smectite layer (10 Å). Overall, the sample is composed of chlorite and low-charge corrensite, which can be partially, interstratified with each other, giving major 14 Å spacing with less 10 Å layers (Fig. 9b). Similar textures were described by Kogure et al. (2013), for their samples, where generally the corrensite–chlorite layers were often curved in their cross-sectional views. Lenticular voids are common in the crystals, which were presumably formed by the collapse of hydrated smectite-like interlayers in the vacuum environment during ion-milling and/or TEM examination. Illite is also present as a minor phase in the sample, as also indicated by the presence of a weak peak at 10 Å in XRD diagrams. Lattice fringes of 20 Å have been recognized in some images, which indicate illite with 2M polytype.

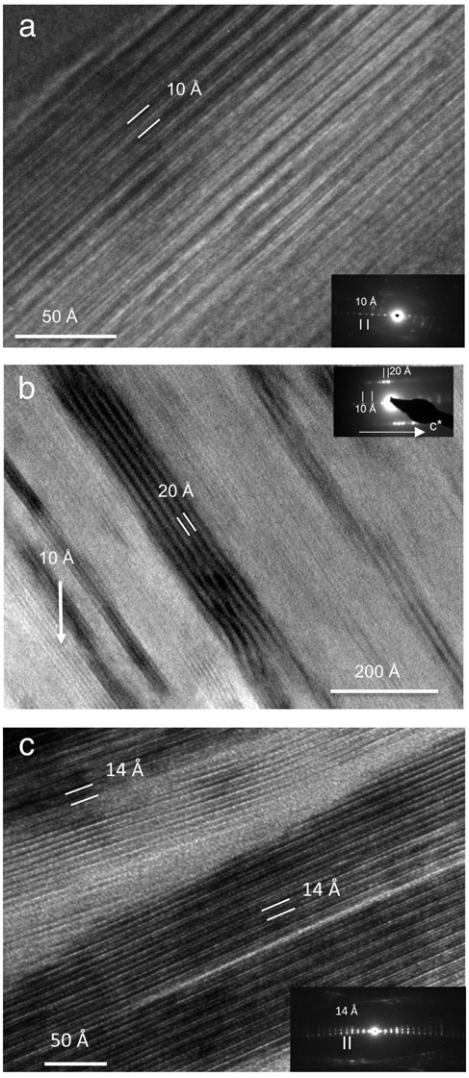

Fig. 8. High magnification images of clay minerals in 653 sample. (a) Illite showing lattice fringes with spacing to 10 Å. SAED pattern corresponds to $1M_d$ polytypism. (b) Lattice fringes with spacing of 10 and 20 Å and SAED pattern corresponding to 2M polytypism in more mature mica. (c) Chlorite with 14 Å layers in 653 sample. SAED pattern corresponds to disordered chlorite polytype.

4.3. Analytical electron microscopy

4.3.1. Smectite and illite–smectite mixed-layers.

Table 1 presents the analyses corresponding to smectite and intermediate illite–smectite compositions. They correspond in all cases to dioctahedral compositions. In some cases, the octahedral sum is slightly higher than normal. Two causes for this are possible; one is that Na could not be determined on copper grid preparations due to the overlapping of the L line of copper, but according to ion milling sample analyses, is present in minor proportions. This deficit of positive charge produces an artificial slight increase of the overall number of cations. The second cause is that a part of Mg, which, in the absence of a valid criterion of distribution, we have totally assigned to the octahedral position, may be also in the interlayer.

Smectite in sample 158 presents more homogeneous compositions than I–S in samples 328 and 653, which considerably overlap their respective fields of composition (Fig. 10). Smectites have the highest Fe and Mg contents, reflecting their montmorillonite–nontronite composition and very limited beidellitic component. The sum of these two elements is similar in samples 328 and 653, but the latter present lower values for some particular analyses (Fig. 10). The ratio between the two elements is different from sample 328 to 653. The major interlayer cation in smectite is Ca.

Samples 328 and 653 have a lower Si content and higher interlayer sums (Fig. 10) in comparison to smectites of sample 158, differences which are coherent with their more illitic composition. Plotted in the Velde (1985) diagram, the three samples show evolution toward a more beidellitic and/or illitic character with increasing depth (Fig. 11). In fact, some of the analyses in sample 653 clearly reach the field of muscovite compositions (Table 1). Nevertheless, the corresponding compositional fields are far to be clearly separated; significant overlap of the fields corresponding to the three samples exists.

Sample 653, characterized by R3 I–S shows the highest K and interlayer cations content and the lowest Si content. Sample 328, containing R1 I–S mixed layer phases, presents an intermediate composition between 158 and 653 (Fig. 10).

The increase of negative tetrahedral charge, linked to Si diminution from more smectitic compositions toward the more illitic ones is basically compensated for by interlayer charge increase. Nevertheless, an additional mechanism for compensation linked to Mg substitution by trivalent cations is also observed on Fig. 10. Therefore, together with the classical $Si^{4+} + \square \rightarrow Al^{3+} + K^{+}$ we find also a $Si^{4+} + Mg^{2+} \rightarrow Al^{3+} + Al^{3+}$ compositional vector, that is, a decrease of tschermack component, which brings the I–S toward more muscovitic compositions. This chemical evolution can be also observed on the Velde (1985) diagram (Fig. 11) by the progressive displacement of the compositions toward the 3R2 + free side of the triangle. In addition to these two chemical changes, also a decrease in Fe content may be observed from the smectitic to the illitic samples.

4.3.2. Chlorite and corrensite

The majority of analyses obtained on major 14 Å areas show mixed characteristics between those of pure chlorite and pure corrensite (Fig. 12). Nevertheless, some extreme analyses produce formulae, which can be considered as pure chlorite (Table 2) and corrensite respectively (Table 3). The rest of the compositions can be considered as

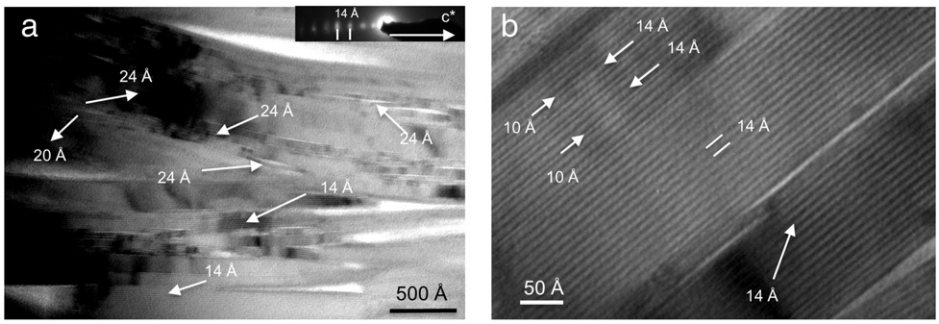

Fig. 9. Chlorite and low-charge corrensite in 776 sample. (a) Layers to 24 Å corresponding to corrensite, are the result of an ordered sum of one chlorite layer (14 Å) and one contracted smectite layer (10 Å). They are intergrowth with 14 Å chlorite layers and 20 Å of illite layers (2M polytype). (b) Layers to 14 Å with minor 10 Å layers showing chlorite intergrowth and/or interstratified with corrensite.

Table 1
Representative AEM analyses of smectites, illites and I/S mixed-layers normalized to $O_{10}(OH)_2$.

	Si	^{IV}Al	^{VI}Al	Fe	Mg	$\sum^{VI}$	Na	K	Ca	$\sum$ inter.
158-1	3.97	0.03	1.01	0.66	0.42	2.08	–	0.09	0.10	0.29
158-2	3.81	0.19	0.79	0.90	0.38	2.08	–	0.09	0.14	0.36
158-3	4.05	0.00	1.00	0.64	0.36	1.99	–	0.00	0.09	0.17
158-5	3.97	0.03	1.01	0.71	0.24	1.96	–	0.07	0.19	0.45
158-8	3.97	0.03	1.01	0.67	0.43	2.11	–	0.03	0.07	0.17
158-11	3.91	0.09	0.91	0.84	0.33	2.09	–	0.05	0.05	0.16
158-12	3.88	0.12	0.88	0.80	0.40	2.08	–	0.07	0.12	0.31
158-13	4.04	0.00	1.05	0.62	0.31	1.97	–	0.05	0.10	0.26
158-14	3.90	0.10	0.98	0.64	0.47	2.09	–	0.09	0.14	0.36
158-15	4.05	0.00	1.01	0.60	0.33	1.94	–	0.03	0.14	0.31
158-16	4.02	0.00	0.85	0.69	0.50	2.04	–	0.05	0.12	0.29
158-19	3.89	0.11	0.96	0.71	0.40	2.06	–	0.05	0.14	0.33
158-20	3.82	0.18	0.82	0.86	0.46	2.14	–	0.02	0.09	0.19
328-2	3.36	0.64	1.45	0.28	0.41	2.14	–	0.51	0.05	0.62
328-3	3.37	0.63	1.58	0.21	0.30	2.10	–	0.55	0.05	0.66
328-4	3.46	0.54	1.58	0.21	0.28	2.07	–	0.49	0.07	0.63
328-5	3.38	0.62	1.47	0.30	0.39	2.15	–	0.41	0.07	0.55
328-6	3.32	0.68	1.65	0.24	0.17	2.07	–	0.31	0.12	0.56
328-7	3.53	0.47	1.69	0.16	0.23	2.07	–	0.33	0.03	0.40
328-8	3.49	0.51	1.45	0.25	0.33	2.03	–	0.46	0.11	0.67
328-22	3.47	0.53	1.61	0.21	0.28	2.09	–	0.33	0.05	0.44
328-23	3.46	0.54	1.66	0.17	0.26	2.09	–	0.37	0.03	0.44
328-26	3.54	0.46	1.64	0.17	0.31	2.13	–	0.28	0.05	0.38
328-28	3.51	0.49	1.70	0.16	0.26	2.11	–	0.24	0.07	0.38
328-29	3.60	0.40	1.64	0.19	0.21	2.04	–	0.31	0.07	0.45
328-30	3.50	0.50	1.59	0.24	0.31	2.14	–	0.28	0.02	0.31
328-1A	3.72	0.28	1.71	0.14	0.21	2.06	0.00	0.21	0.10	0.41
328-2A	3.93	0.07	1.81	0.00	0.19	2.00	0.00	0.09	0.09	0.26
328-3A	3.69	0.31	1.72	0.00	0.34	2.06	0.00	0.21	0.11	0.42
328-4A	3.67	0.33	1.78	0.00	0.27	2.05	0.00	0.25	0.07	0.39
328-5A	3.77	0.23	1.67	0.19	0.26	2.12	0.00	0.21	0.07	0.34
328-6A	3.49	0.51	1.53	0.25	0.29	2.06	0.12	0.62	0.04	0.81
328-7A	3.66	0.34	1.67	0.21	0.19	2.08	0.00	0.35	0.07	0.49
328-8A	3.67	0.33	1.57	0.19	0.26	2.02	0.10	0.38	0.09	0.66
653-2	3.20	0.80	1.78	0.14	0.13	2.05	–	0.83	0.07	0.96
653-3	3.48	0.52	1.90	0.00	0.11	2.01	–	0.71	0.00	0.71
653-5	3.62	0.38	1.49	0.36	0.31	2.15	–	0.59	0.09	0.75
653-6	3.53	0.47	1.38	0.44	0.27	2.09	–	0.59	0.12	0.82
653-8	3.49	0.51	1.67	0.23	0.25	2.15	–	0.53	0.02	0.56
653-9	3.52	0.48	1.70	0.25	0.25	2.20	–	0.44	0.05	0.54
653-11	3.35	0.65	1.83	0.13	0.05	2.01	–	0.79	0.04	0.85
653-12	3.31	0.69	1.80	0.19	0.11	2.10	–	0.64	0.00	0.63
653-14	3.35	0.65	1.85	0.00	0.27	2.13	–	0.89	0.00	0.88
653-16	3.28	0.72	1.88	0.11	0.11	2.09	–	0.57	0.02	0.60
653-30	3.62	0.38	1.72	0.14	0.21	2.07	–	0.44	0.03	0.51
653-31	3.65	0.35	1.43	0.42	0.33	2.18	–	0.46	0.00	0.45
653-32	3.50	0.50	1.50	0.35	0.21	2.07	–	0.76	0.05	0.86
653-33	3.46	0.54	1.78	0.14	0.19	2.12	–	0.37	0.05	0.47
653-1A	3.33	0.67	1.77	0.07	0.12	1.96	0.39	0.30	0.11	0.90
653-2A	3.38	0.62	1.75	0.07	0.12	1.95	0.37	0.32	0.11	0.90
653-3A	3.26	0.74	1.83	0.09	0.11	2.02	0.23	0.44	0.04	0.74
653-4A	3.85	0.15	1.88	0.07	0.07	2.02	0.00	0.12	0.05	0.22
653-5A	3.52	0.48	1.87	0.11	0.07	2.05	0.18	0.19	0.04	0.44

corresponding to chlorite–corrensite mixed layers, that is, compositions with a number of 14 Å layers intermediate between 50% and 100%. In such cases the right number of oxygen atoms to be considered in the formula calculation would depend on the exact proportion of chloritic and smectitic/vermiculitic layers, hence it is different and unknown for each analysis, which precludes the conversion of such compositions in mineral formulae.

Corrensite composition (Table 3 and Fig. 12) is highly heterogeneous at the level of the sample, and from sample to sample. Overall octahedral sums approach 9, therefore, presumably, it is trioctahedral, for the two components; however they show some minor variable deficits, which are higher for sample 328 than for 776. The Fe and Mg contents are similar to each other and high, with no significant differences between the samples. Sample 776 presents clearly lower Al content and generally higher Si content than 328. The interlayer sum is similar between the two samples, but the major interlayer cation is K for sample 328, while Ca is clearly predominant in 776.

Chlorite also displays a very heterogeneous composition (Table 2 and Figs. 12 and 13). The majority of the analyses show high Si content and low octahedral sums, both typical characteristics of low temperature chlorites (Vidal et al., 2005; Inoue et al, 2009). Nevertheless, some significant exceptions may be found, with the two chemical parameters clearly different from the general tendency of the sample (Fig. 13 and Table 2). No clear relationship exists between such differences and a possible contamination by dioctahedral phases, evaluated through the interlayer cation content of each individual analysis (Table 2). In general Mg content is slightly higher than Fe, with no clear differences among the three samples.

In the R2 + -Si diagram of Wiewióra and Weiss (1990) most of the chlorite compositions concentrate between the clinochlore, sudoite and corundophullite, though some extension was observed toward Al-free chlorite (Fig. 13). However, corrensites show clearly different compositions, significantly closer to sudoite.

5. Discussion

5.1. The vertical distribution of clay minerals

Different clay mineral assemblages have been recognized along the Pte-1 drill hole from the Tinguiririca geothermal field in the Andean Cordillera of central Chile, which have allowed us to organize them in four main clay mineral alteration zones: (1) alteration zone I (from 0 to 300 m) dominated by smectite, (2) alteration zone II (from 300 to 410 m) dominated by R1 I–S mixed layers, chlorite and high-charge corrensite; (3) alteration zone III (from 410 to 700 m) dominated by R3 I–S mixed layers, chlorite and high-charge corrensite; (4) alteration zone IV dominated by low-charge corrensite and chlorite.

The smectite to illite sequence is discontinuous, according to XRD. A smectite-rich I–S zone between zone 1 (smectite) and zone 2 (R1) has not been identified. TEM data also agree with XRD. We have not identified R0 I–S, whose major component was smectite. Therefore, apparently the change from alteration zones I to II is discontinuous. Nevertheless, a more exhaustive sampling of this part of the sequence would be useful to clarify this point.

5.1.1. Smectite and I–S mixed layer zones: I–S formation

The shallow zone is characterized by the presence of aluminous clay phases (smectite, scarce berthierine, and I–S mixed layers) associated with pyrite, and hematite. The clay mineral assemblages developed at 158 m consist mostly of smectite. The chemical composition of the smectite is coherent with a montmorillonite with high nontronitic component and very low beidellitic component. Such composition is typical of smectites related with a significant volcanic input, such as an early alteration product of volcanic glass (eg. Bauluz et al., 2000, 2002; Guisseau et al., 2007).

Regularly ordered I–S mixed layers have been identified from 325 m to 661 m. The content in expandable layers of this I–S mixed layers decreases with the depth and temperature, indicating a prograde reaction of smectite to illite via I–S mixed layers, in the presence of near neutral geothermal waters (Reyes, 1990). The reaction of smectite to illite, via I–S mixed layers has been widely reported in hydrothermal and diagenetic systems. Previous studies of I–S minerals suggested an illitization sequence, which was apparently continuous from smectite through I–S phases to illite (eg. Harvey and Browne, 1991). This transition of smectite to illite has been considered as the result of a thermally active sequential transformation reaction from smectite precursor to illite which proceeds via crystallization of I–S mixed layers series (Meunier and Velde, 1989) or as a result of simultaneous crystallization of all the I–S mixed layers via direct precipitation from solution (Inoue et al., 2004). In the Tinguiririca geothermal fields, the variation in the

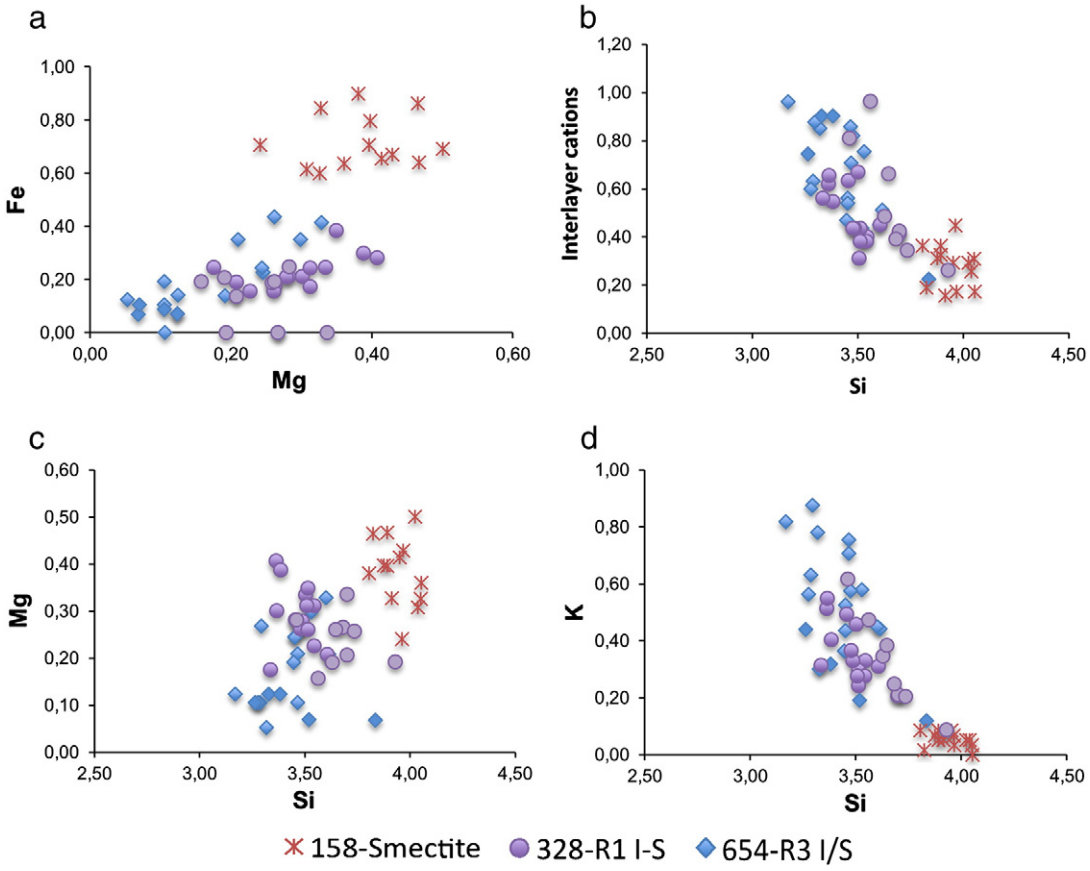

Fig. 10. Compositional diagram of AEM analyses corresponding to smectite, and I–S mixed layers from 158, 328 and 653 samples. (a) Mg vs Fe. (b) Si vs Interlayer cations. (c) Si vs Mg. (d) Si vs K.

proportions of smectite (S) and illite (I) layers in the I–S minerals can be correlated directly with the temperature.

The textural evidences of clay minerals under TEM and in addition to the thin-section observations, indicate that primary minerals were in part dissolved by hydrolytic reaction and the smectite and I–S mixed layers precipitated *in situ* from the altering solutions. The typical defective characteristics of smectite, with layer terminations, dislocations,

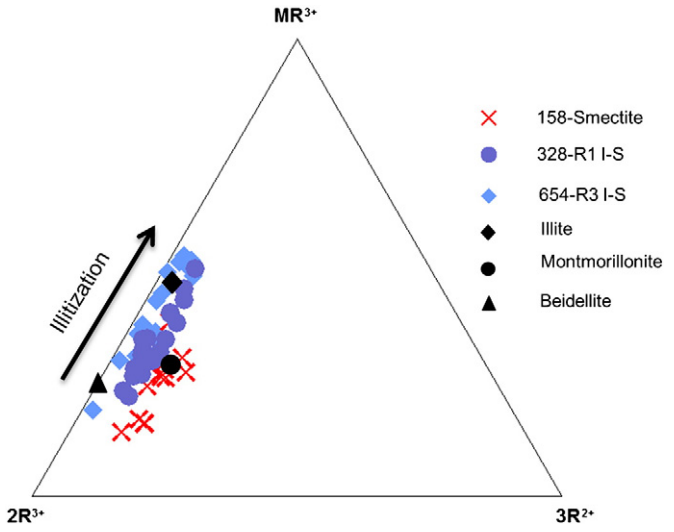

Fig. 11. Compositional diagram MR3- 2R3-3R2 (Velde, 1985) of the smectite and I–S mixed layers AEM analysis. MR3+: (Na+ + K+ + 2Ca2+), 2R3+: (Al3+ + Fe3+ − MR3+)/2, 3R2+: (Fe2+ + Mg2+ + Mn2+)/3.

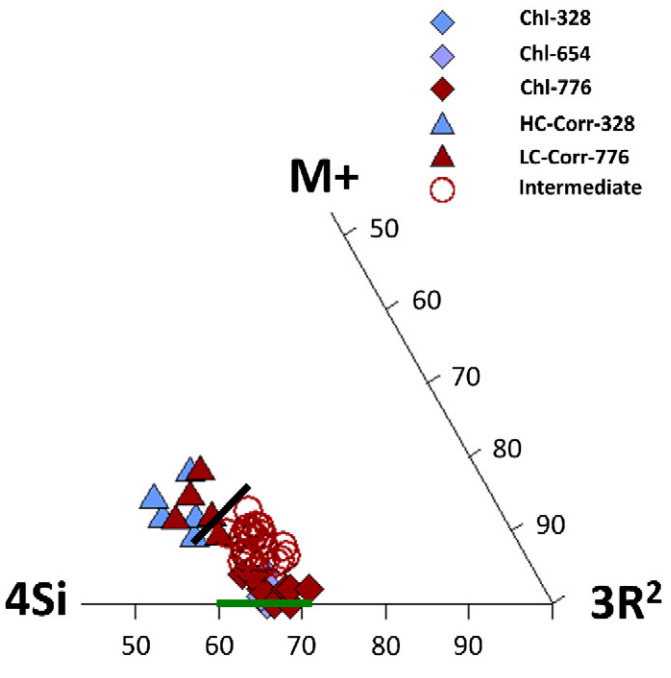

Fig. 12. Compositional diagrams M^{+}-4Si-$3R^{2+}$ (Meunier and Velde, 1989) of chlorite, corrensite and intermediate mixed layers of C–S and C–V (more than 50% of chlorite). Theoretical chlorite composition is given by green line and theoretical 50–50 corrensite composition is plotted by black line (Meunier et al., 1991). $M^{+} = Na^{+}, K^{+}, 2Ca^{2+}$; 4Si = Si/4; $3R^{2+} = (Mg^{2+} + Fe^{2+} + Mn^{3+})/3$.

Table 2
Representative AEM analyses of chloritic phases normalized to $O_{10}(OH)_8$.

	Si	^{IV}Al	^{VI}Al	Fe	Mg	Mn	$\sum^{VI}$	K	Na	Ca	$\sum$inter.
653-17*	3.08	0.92	1.33	1.70	2.77	–	5.80	0.07	–	0.00	0.07
653-18*	3.04	0.96	1.39	1.50	2.90	–	5.78	0.00	–	0.00	0.00
653-22**	3.17	0.83	1.39	1.77	2.55	–	5.72	0.00	–	0.07	0.14
653-6A**	2.87	1.13	1.67	2.32	1.74	–	5.73	0.03	0.20	0.00	0.23
653-8A**	2.99	1.01	1.43	2.80	1.57	–	5.79	0.07	0.00	0.10	0.27
653-9A**	3.12	0.88	1.38	2.09	2.28	–	5.75	0.02	0.00	0.00	0.02
653-10A**	2.92	1.08	1.65	2.56	1.51	–	5.72	0.10	0.00	0.00	0.10
653-13A**	3.09	0.91	1.04	2.12	2.77	–	5.94	0.00	0.00	0.07	0.14
653-14A*	2.75	1.25	1.01	2.31	2.80	–	6.12	0.00	0.00	0.02	0.05
776-1**	3.07	0.93	1.24	2.27	2.34	–	5.85	0.05	–	0.10	0.24
776-2*	3.12	0.88	1.34	2.19	2.24	–	5.77	0.00	–	0.02	0.05
776-3*	3.20	0.80	1.48	1.92	2.25	–	5.66	0.00	–	0.05	0.09
776-4**	3.04	0.96	1.25	2.29	2.31	–	5.86	0.00	–	0.12	0.24
776-5**	3.19	0.81	1.24	2.30	2.25	–	5.78	0.10	–	0.12	0.34
776-6**	3.22	0.78	1.26	2.02	2.48	–	5.76	0.02	–	0.12	0.26
776-7**	3.07	0.93	1.23	2.23	2.38	–	5.85	0.05	–	0.05	0.14
776-9**	2.99	1.01	1.35	2.27	2.22	–	5.83	0.07	–	0.10	0.27
776-10**	2.85	1.15	1.29	2.17	2.46	–	5.93	0.00	–	0.07	0.14
776-11*	3.03	0.97	1.30	2.20	2.34	–	5.83	0.00	–	0.00	0.00
776-12*	2.90	1.10	1.23	2.14	2.57	–	5.93	0.00	–	0.02	0.05
776-13**	2.99	1.01	1.38	1.89	2.54	–	5.81	0.05	–	0.05	0.14
776-14*	2.93	1.07	1.16	2.16	2.64	–	5.96	0.00	–	0.00	0.00
776-15**	3.16	0.84	1.32	2.25	2.18	–	5.76	0.07	–	0.07	0.22
776-16**	2.76	1.24	1.30	2.13	2.54	–	5.97	0.05	–	0.07	0.19
776-17*	3.29	0.71	1.24	2.17	2.33	–	5.74	0.00	–	0.05	0.10
776-18**	3.24	0.76	1.33	2.04	2.35	–	5.72	0.05	–	0.10	0.24
776-20**	3.24	0.76	1.33	2.04	2.35	–	5.72	0.05	–	0.10	0.24
776-2A**	3.20	0.80	1.40	2.25	2.05	–	5.70	0.02	0.00	0.07	0.17
776-4A**	3.02	0.98	1.30	2.10	2.44	–	5.84	0.00	0.00	0.10	0.19
776-5A**	3.21	0.79	1.29	2.37	2.10	–	5.75	0.02	0.00	0.12	0.27
776-6A**	3.20	0.80	1.41	2.24	2.04	–	5.69	0.00	0.00	0.10	0.19
776-7A**	3.32	0.68	1.31	2.06	2.32	–	5.68	0.00	0.00	0.07	0.14
776-8A**	3.43	0.57	1.39	2.06	2.13	–	5.59	0.00	0.00	0.12	0.24
776-10A**	3.25	0.75	1.26	2.34	2.08	0.07	5.75	0.00	0.00	0.07	0.14
776-11A**	2.93	1.07	1.05	2.66	2.22	0.07	6.01	0.02	0.00	0.07	0.17
776-12A*	2.87	1.13	1.20	2.60	2.12	0.05	5.97	0.00	0.00	0.02	0.05
776-17A**	3.20	0.80	1.20	2.24	2.31	0.05	5.80	0.00	0.00	0.07	0.14
776-13A**	3.09	0.91	1.04	2.12	2.77	–	5.94	0.00	0.00	0.02	0.05
776-14A**	2.75	1.25	1.01	2.31	2.80	–	6.12	0.00	0.00	0.60	1.20
776-17A**	3.20	0.80	1.08	2.38	2.41	–	5.86	0.07	0.00	0.07	0.22
328-15*	2.95	1.05	1.44	2.13	2.23	–	5.80	0.05	0.00	0.02	0.10

* Chlorites.
** Chlorites mixed layer.

contrast changes, are also observed in the I–S mixed layers (Figs. 5 and 7a and b) indicating that these phases are involved in the prograde reaction. This reaction was detected from 325 to 408 m, where ash-dominated volcanic rocks are cut by the borehole. It is known that solutions reacting with vitric materials at a given temperature might increase in pH and dissolved solids, enriching the solution in Mg, Ca and Na as well as SiO_2. The resulting high pH and Na solution favors the formation of smectite (eg. Hay and Sheppard, 2001; Inoue et al., 2004). Due to a higher temperature in the 325–408 m intervals, the hydrolytic reaction forms aluminous I–S minerals instead of montmorillonite by incorporating K ions into the structure from ambient solutions.

Table 3
Representative AEM analyses of corrensites normalized $O_{20}(OH)_{10}$.

	Si	^{IV}Al	^{VI}Al	Fe	Mg	Mn	$\sum^{VI}$	K	Ca	$\sum$inter.
328-12	6.18	1.82	3.02	2.57	2.82	–	8.40	0.29	0.08	0.46
328-14	6.04	1.96	2.45	3.26	3.04	–	8.75	0.21	0.30	0.81
328-16	6.09	1.91	2.46	3.03	3.24	–	8.72	0.13	0.13	0.38
328-19	6.47	1.53	2.92	2.61	2.77	–	8.30	0.34	0.13	0.59
328-20	6.18	1.82	2.29	3.09	3.39	–	8.77	0.17	0.17	0.51
776-8	6.19	1.81	1.88	3.31	3.77	–	8.96	0.13	0.21	0.55
775-1A	6.14	1.86	1.79	3.52	3.73	–	9.03	–	0.21	0.42
776-3A	6.44	1.56	2.12	3.51	3.09	–	8.72	–	0.34	0.68
776-9A	6.69	1.31	2.26	3.15	3.03	0.08	8.53	–	0.25	0.50
776-13A	6.42	1.58	1.79	3.34	3.76	–	8.89	0.04	0.43	0.90

5.1.2. R3 I–S zone

The following zone is characterized by the presence of illite rich I–S, corrensite and chlorite as the main phyllosilicates and Ca-silicates (wairakite, prehnite, epidote and titanite). The illite in this zone corresponds to an illitic phase with low expandable component (<10% of smectite). The HRTEM data show that the sample at 653 m is composed of intergrowths of illite and chlorite. At this depth, the illite has straight boundaries and defect-free lattice fringes indicating a lower defective character than those formed in the shallower parts. The illite polytype observed are $1M_d$ and 2M. Therefore, at this depth the illite features are typical of higher temperatures. The existence of differences of composition between the areas which show SAED typical of $1M_d$ and 2M polytypes could indicate the beginning of the transition from the R3 I–S zone to the illite *sensu stricto* zone, with coexistence of the two kinds of illitic materials, showing differences in polytype and composition. In fact, some typical analyses corresponding to mature micas may be found in Table 2 (e.g. 653-2, 653-1A and 653-2A). The coexistence of various types of I–S materials at the sample level is a proven fact, frequently described in the literature (e.g. Nieto et al., 1996; Ferrage et al., 2011).

5.1.3. Corrensite and chlorite: corrensite formation

The mineral assemblages of altered rocks below 735 m until the bottom of the borehole reveal the presence of low-charge corrensite and

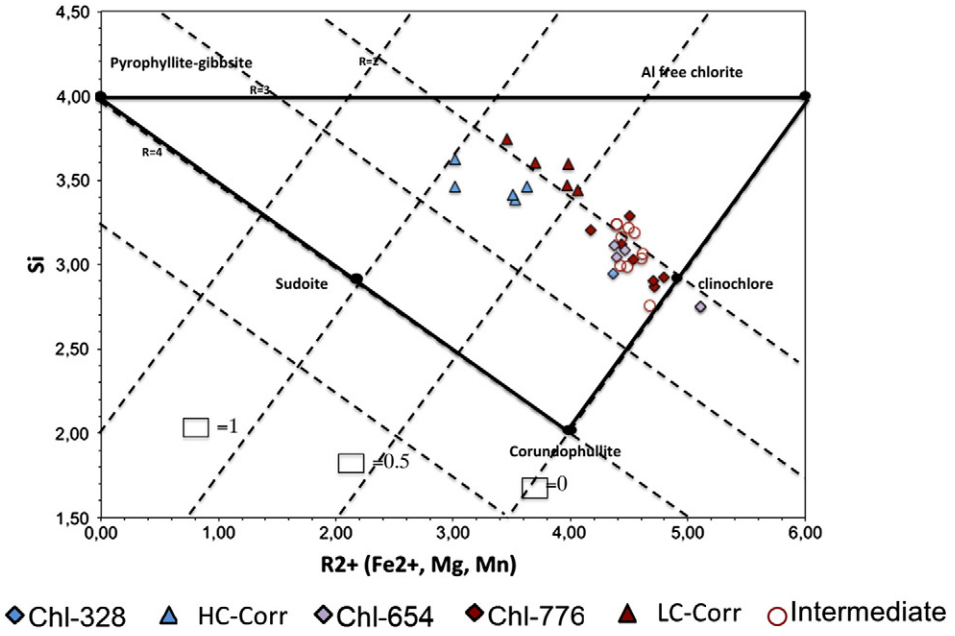

Fig. 13. Chemical compositions of chlorites from Tinguiririca geothermal field plotted in the R2 + -Si diagram of Wiewióra and Weiss (1990); all Fe considered as Fe(II).

chlorite. The transition of smectite to chlorite consists of the formation of chlorite–smectite (C–S) irregularly mixed layered (e.g. Bettison et al., 1991; Schiffman and Fridleifsson, 1991; Robinson and Bevins, 1994; Meunier et al., 2008a,b; Leoni et al., 2010) or discontinuous changes from smectite to corrensite to chlorite without irregularly mixed-layered chlorite–smectite (e.g. Inoue et al., 1984; Shau et al., 1990; Inoue and Utada, 1991; Schiffman and Staudigel, 1995; Beaufort et al., 1997; Schmidt and Robinson, 1997). The increase in chlorite content often is related with an increase in temperature (Schiffman and Fridleifsson, 1991). Corrensite occurs between 100 and 200 °C (Inoue and Utada, 1991). The complete change of corrensite to discrete chlorite is completed above 240 °C (e.g. Kristmannsdótti, 1976; McDowell and Elders, 1980, Keith and Bargar, 1988). High chlorite content can also be related to high fluid/rock ratio or mineral alterations, which provide the Al needed to form chlorite (Shau and Peacor, 1992; Schmidt and Robinson, 1997).

Low-charge corrensite and discrete chlorite in our samples appear at temperatures measured in the borehole of 220 °C. This temperature is too high for the stability field of corrensite. However, the application of the Bourdelle geothermometer in chlorites from sample 776 indicates a temperature of formation for one group of chlorites around 140 °C, which is perfectly coherent with the presence of low-charge corrensite and chlorite in sample 776. Therefore, in the Tinguiririca samples the presence of corrensite at the bottom of the borehole shows that the alteration temperature was lower than the present-day temperature.

5.2. Chemical evolution of I–S

The knowledge of the chemistry of I–S phases and the limits of their compositional fields has been hindered by their defective character, small size and lack of adequate analytical methods. Consequently, their compositional fields are still obscure and a lack of a definition of typical chemical compositions still exists in the mineralogical literature, which does not allow their unambiguous identification based only on their chemical composition.

The presented results for the Tinguiririca borehole Pte-1 offer an opportunity to extend the knowledge of the chemical compositions and evolution with temperature and depth of their chemistry. The mineralogy is relatively simple, with virtual absence of detrital phases and the calculated formulae are based on high quality analyses. We have combined two kinds of preparations of samples to have the opportunity of referring the obtained compositions to given textural positions and high-resolution images and, at the same time, using the best possible analytical conditions in AEM (see Methods section). The two kinds of analyses have defined the same compositional fields for each of the studied samples with no significant differences in relation to the two kinds of preparations (compare in Table 1 the formulae labeled with A, after the number, obtained on ion-milled samples with those without A, obtained on grid samples). A former version of Figs. 10 and 11, differentiating the two kinds of analyses (not shown, for simplicity) showed no-difference between them. Therefore we are confident that the overall set of analyses represents the corresponding phases shown in the high-resolution images and, at the same time, offers the maximum analytical quality that the currently available methods can offer.

Given the respective chemical composition of smectite and illite and the partial former results about the I–S chemistry, it has been assumed that more mature I–S should be characterized by a diminution of the pyrophyllitic component toward a theoretical muscovite. In other words, we could expect illite-richer I–S higher interlayer charge, particularly related with K increase, which balances a diminution of the tetrahedral charge due to the increase of Al and decrease of Si. The Tinguiririca results, shown in Fig. 10, perfectly confirm this broad tendency and can be considered as conclusive for such a prediction.

Nevertheless, when the results presented on Fig. 10 are considered in detail, we can establish two refinements to this general conclusion. The first one is the existence of a second chemical balance which compensates the Si decrease in addition to the diminution of the pyrophyllitic component, based on a coeval decrease of the tchermack component, that is, a substitution of Mg + Fe by Al in the octahedral layer. The second one is the highly heterogeneous character of the compositional fields of the implied phases. The respective fields of compositions broadly overlap each other, making a definition of differentiated fields for each of the types of I–S mixed layers impossible. In other words, I–S mixed-layer types cannot be distinguished based only on chemical compositions.

5.3. Relationship between measured temperature and I–S mineral changes

Many authors have focused their studies on establishing the temperatures of the transformations in the system smectite-I–S-illite. Generally,

the temperatures where I–S mixed layers R1 with approximately 50%–60% of illite layers appears in diagenetic environments are in the range from 75 to 120 °C (Hoffman and Hower, 1979; Srodon and Eberl, 1984; Schegg and Leu, 1996; Uysal et al., 2000; Abid et al., 2004). Libbey et al. (2013) also showed a positive correlation between the proportion of illite in the I–S interlayer and downhole temperature in the Te Mihi area, Wairakei geothermal field (New Zealand), even suggesting a local I–S geothermometer based on the illite proportion. In the Tinguiririca borehole the last smectite sample corresponds to a temperature of 80 °C and the first one in which this last has been replaced by R1 I–S to 120 °C. Therefore, a temperature around 100 °C, perfectly compatible with the previous range defined in the literature, may be considered as a valid reference for this first step of the transformation from smectite to illite.

The transition from R1 to I–S R3 with more than 85% of illite layers has been described in the diagenetic literature at 150–190 °C (Hoffman and Hower, 1979; Weaver, 1989; Lindgreen, 1991; Pollastro, 1993; Abid et al., 2004). In our case, I–S mixed layers appear with R3 ordering and 90% of illite layers at 408 m. The measured temperature in the borehole was of 125 °C at 325 m, suddenly increasing to 180 °C at 408 m. Therefore the temperature of the sequence of increasing illite and ordering of I–S mixed layers agrees well with the temperature previously exposed.

Previous comparisons are based on the extensive literature about diagenetic environments. The extent at which they can be extended to a hydrothermal environment is unknown. Some papers have emphasized the fact that the different steps of the transformation process can be retarded in terms of temperature by scarce disposability of reactants due to lack of porosity and low K content. For example, Arostegui et al. (2006) found temperatures of 160 °C for the disappearance of smectite and 240 °C for the R1-R3 transition in marly lithologies. As an opposite case, the open crystallization from a fluid rich in the illite components in a geothermal field offers an ideal environment for the transformation. Other geological environments, as with the diagenetic one, could increase such temperatures due to local factors.

Finally, it is highlighted that the transformation into pure illite has not been completed at the bottom of the borehole, with some minor residual smectitic layers even at temperatures as high as 220 °C. The difficulty of the completeness of the reaction based only on thermal effects, without tectonically induced strain as a driving force for the reaction, is a widely accepted fact in the incipient metamorphism literature (Merriman and Peacor, 1999).

5.4. Chlorite thermometry

Discrete chlorite displays a wide range of non-stoichiometric compositional variations depending on bulk rock composition and physicochemical conditions prevalent at the formation. The variation of chemical composition in chlorite therefore is useful to obtain information on the physicochemical conditions of the formation, such as the temperature. However, chlorite geothermometry has been a widely controversial matter during years (Cathelineau, 1988; de Caritat et al., 1993; Lopez-Munguira et al., 2002; Vidal et al., 2005, 2006; Inoue et al, 2009). The first geothermometers proposed by Cathelineau and Nieva (1985) and Cathelineau (1988) were based on direct empirical relationships between some chemical parameters and measured temperatures in geothermal areas (Los Azufres, Mexico), but it was questioned that they were widely affected by small scale interstratifications and intergrowths and are not based on chemical equilibrium (Essene and Peacor, 1995). Therefore, the empirical relationship was only valid for the studied geological context. The introduction of Vidal and Inoue's thermodynamic geothermometers based on the overall composition of chlorite was a significant step. Nevertheless, their wide use was severely limited by the necessity of the Fe^{2+}/Fe^{3+} ratio of the chlorite, which is difficult for low temperature materials. Recently, Bourdelle et al. (2013) have published a new semi-empirical chlorite geothermometer, which does not require prior Fe^{3+} knowledge, calibrated on 161 analyses with well-constrained T data covering a wide range of geological contexts and tested for low-T chlorites (T <350 °C and pressures below 4 kbar).

We have applied the Bourdelle geothermometer to Tinguiririca chlorite phases. According to the Bourdelle et al. (2013) recommendation, chlorite must be free of 10 Å layers. We have then limited the application of the geothermometer only to analyses producing formulae with less than 0.10 interlayer charge. Fig. 2 compares the obtained temperatures with those directly measured in the borehole.

In broad outlines, some differences have been observed between the empirical temperatures calculated using chlorite chemical composition and the present day measured temperatures. The temperature obtained with the geothermometer in sample 328 is 178 °C, which represents a difference with the temperature measured in the borehole of around 50 °C, which is the error margin of the Bourdelle geothermometer. Two temperatures calculated for sample 653 (653-17 and 653-18) are exactly the same as the average temperature of the borehole at this depth. The temperature calculated using the 653-9A analysis is only 46 °C lower than the average temperature in the borehole, being the difference also under the predicted error limits of the method.

Finally, the highest differences were obtained in sample 776 (bottom of the drill core). In fact, in this sample we can recognize two well defined groups of temperatures, which are clearly different to the 233 °C of the measured temperature of the borehole at this depth. One group has an average temperature of 139 °C and the other 346 °C. These two groups of temperatures are the consequence of two groups of chlorites in the sample with very different morphology and compositions (Figs. 12 and 13). One of the groups shows the chemical characteristics invoked by all the thermometric approaches for low temperature chlorites, that is, high Si and low octahedral population, being coincident with the chemical character of the rest of samples of the borehole. The other group of compositions shows just the opposite characteristics and, therefore, would produce higher temperatures independently of the used thermometric model. Hence, if we accept the thermodynamic basis of the chlorite thermometry, we need to admit the existence of two groups of chlorites in the sample formed at clearly different temperatures. These two chlorite groups were then formed during two different alteration events along the evolution of the Tinguiririca geothermal field. Moreover, the chlorites of lowest temperatures would be not in equilibrium with hydrated Ca-Al silicates (wairakite, epidote and prehnite) observed in the lower part of the core with the temperature of formation normally higher than that calculated by means of chlorite thermometry for this group of analyses. Wairakite is normally described in geothermal systems worldwide to be stable in the 200°–300 °C interval, meanwhile epidote and prehnite are normally stable over 200 °C (e.g. Browne, 1978; Henley and Ellis, 1983; Reyes, 1990). Gas geochemistry geothermometry (H_2-Ar, CO_2-Ar and CO_2-CH_4) suggests equilibration temperatures in between 220° and >300 °C for reservoir conditions (Clavero et al., 2011), in concordance with the highest temperatures obtained using chlorite thermometry and propylitic alteration mineralogy. Consequently, the low-T chlorite group could be in relation with the cooling of the system by cold water influx, as reflected by the present day measured temperature. Moreover, at these depths abundant hematite in veins is frequently observed (some of then centimetric in width) and clots in the matrix, interpreted by Reyes (1990) as indicative of cold water input into the geothermal system.

In any case, the persistence of two morphologically and chemically contrasted chlorite families indicates disequilibrium conditions and must be related with the kinetics of the alteration processes in geothermal systems. Contrary to diagenetic processes related to burial, geothermal alteration in active systems is related to rapid events that could preclude the achievement of equilibrium conditions. Similar kinetic constraints were also previously proposed by Inoue et al (2004) to explain differences between present-day temperatures in geothermal

systems and alteration mineral assemblages. Moreover, these authors remarked on the influence of the geologically short period of time during geothermal alteration and different fluids and processes involved in geothermal systems (boiling, mixing) in contrast to burial diagenesis. All these parameters are potentially misleading in terms of the relationship between the observed mineral assemblages and present-day temperature.

Consequently, we tentatively hypothesize that the temperatures around 346 °C could be related with chlorites crystallized during the main alteration event affecting the Tinguiririca geothermal system. This high temperature event is consistent with the alteration mineralogy observed and estimations of reservoir temperature using gas and fluid geochemistry (Clavero et al., 2011). Continuous clay mineral evolution described from top to bottom of the studied core is also consistent with this increasing temperature with depth. On the contrary, the lower temperatures obtained, around 139 °C, could indicate that these chlorites do not reflect the main hydrothermal event and could be related to a cold water influx locally affecting the geothermal system. More detailed studies concerning textural relationships between these two chlorites are necessary with the aim to identify the precise origin of them and define if low T chlorites developed over high-T ones or directly precipitated from hydrothermal fluids.

6. Conclusions

This study contributes to a better knowledge of the vertical distribution of the clay minerals assemblages close to 900 m below the surface area of the geothermal field of Tinguiririca in the Andean Cordillera of central Chile. The evolution with depth of clay mineralogy in this geothermal field is temperature-dependent and consistent with the classical pattern widely described in the hydrothermal and diagenetic literature. Moreover, the clay mineral evolution observed is also consistent, in general terms, with the present day temperature measured in the borehole. Clay minerals grew from solutions enriched in the necessary chemical components by the dissolution of pre-existing volcanic minerals and glass. Montmorillonitic smectite, at the top, evolved to R1 I–S at temperatures around 100 °C and to R3 I–S at nearly 150 °C. The concomitant chemical evolution implied two main compositional vectors toward an end-member muscovitic composition; the major one is the diminution of a pyrophyllitic component ($Si^{4+} + \square \rightarrow Al^{3+} + K^{+}$), with some additional contribution of the reduction of the tschermack component ($Si^{4+} + Mg^{2+} \rightarrow Al^{3+} + Al^{3+}$). Associated to the advent of R1 I–S, Mg released by the latter reaction allowed the onset of chlorite, corrensite and corresponding chlorite–vermiculite mixed-layers, which persist to the bottom of the borehole. The application of the semi-empirical chlorite geothermometer, newly developed by Bourdelle et al (2013) allows the determination of the alteration temperature conditions and contrasts with the present day temperature measured in the borehole. A general trend of increasing temperature with depth has been observed. However, in samples from the bottom of the drill hole, two populations of chlorite with diverse morphology, chemistry, calculated temperature and origins could be differentiated. The origin of these two chlorite families could be related to two different alteration events and the persistence of chlorites with different temperatures reflects disequilibrium conditions controlled by kinetic processes. The highest T chlorite could reflect the real thermal conditions during the main geothermal alteration and could indicate the minimum temperature of the reservoir conditions.

This investigation shows the importance of the study of clay minerals for geothermal exploration and evaluation of the future evolution of geothermal systems. Moreover, the combination of XRD and HR-TEM-AEM techniques gives fast and very reliable characterization of the different clay assemblages and allows the characterization of different clay minerals parageneses that could be related to different geothermal events. Only using high resolution techniques could make possible the identification of different clay mineral generations, allowing the development of alteration models for active geothermal systems.

Acknowledgements

Authors thank Energia Andina company and, especially German Pineda and Richard Sutil, for the facilities in the access to the Pte-1 borehole samples. We also thank M.M. Abad (CIC, University of Granada) for her help with the HRTEM work. Financial support was provided by the Chilean Research Projects Fondecyt-Regular-1140629 and FONDAP-CONICYT-15090013 “Andean Geothermal Center of Excellence (CEGA)”. We are grateful to M. Do Campo for her help in the calculation of chlorite geothermometry. Lucy McGee is acknowledged for reviewing the English. Comments and suggestions from Dr. A. Inoue, Dr. J. Moore and an anonymous referee strongly improved the previous version of the Ms.

References

Abad, I., Mata, P., Nieto, F., Velilla, N., 2001. The phyllosilicates in diagenetic-metamorphic rocks of the South Portuguese Zone, southwestern Portugal. Can. Mineral. 39, 1571–1589. http://dx.doi.org/10.2113/gscanmin.39.6.1571.

Abad, I., Nieto, F., Gutiérrez-Alonso, G., 2003a. Textural and chemical changes in slate-forming phyllosilicates across the external-internal zones transition in the low-grade metamorphic belt of the NW Iberian Variscan Chain. Schweiz. Mineral. Petrogr. Mitt. 83, 63–80. http://dx.doi.org/10.5169/seals-63136.

Abad, I., Nieto, F., Peacor, D.R., Velilla, N., 2003b. Prograde and retrograde diagenetic and metamorphic evolution in metapelitic rocks of Sierra Espuña (Spain). Clay Miner. 38, 1–23. http://dx.doi.org/10.1180/0009855033810074.

Abad, I., Nieto, F., Gutierrez-Alonso, G., Do Campo, M., Lopez-Munguira, A., Velilla, N., 2006. Illitic substitution in micas of very low-grade metamorphic clastic rocks. Eur. J. Mineral. 18, 59–69. http://dx.doi.org/10.1127/0935-1221/2006/0018-0059.

Abad-Ortega, M.D., Nieto, F., 1995. Extension and closure of the compositional gap between Mn-rich and Mg-rich chlorites toward Fe-rich compositions. Eur. J. Mineral. 7, 363–367 (0935-1221/95/0007-0363).

Abid, I.A., Hesse, R., Harper, J.D., 2004. Variations in mixed-layer illite/smectite diagenesis in the rift and post-rift sediments of the Jeanne d'Arc Basin, Grand Banks, offshore Newfoundland, Canada. Can. J. Earth Sci. 41, 401–429. http://dx.doi.org/10.1139/E04-004.

Aguirre, L., Robinson, D., Bevins, R.E., Morata, D., Vergara, M., Fonseca, E., Carrasco, J., 2000. A low-grade metamorphic model for the Miocene volcanic sequences in the Andes of central Chile. N. Z. J. Geol. Geophys. 43, 83–93. http://dx.doi.org/10.1080/00288306.2000.9514871.

Arcos, R., Charrier, R., Munizaga, F., 1988. Volcanitas cuaternarias en la hoya superior del Río Tinguiririca (34°40' Lat S – 70°21' Long W): características geológicas, antecedentes geoquímicos y geocronológicos. V Congreso Geológico Chileno, Tomo III, pp. 1254–1260.

Árkai, P., Merriman, R.J., Roberts, B., Peacor, D.R., Tóth, M., 1996. Crystallinity, crystallite size and lattice strain of illite-muscovite and chlorite: Comparison of XRD and TEM data for diagenetic to epizonal pelites. Eur. J. Mineral. 8, 1119–1137.

Árkai, P., Mata, M.P., Giorgetti, G., Peacor, D.R., Tóth, M., 2000. Comparison of diagenetic and low-grade metamorphic evolution of chlorite in associated metapelites and metabasites: An integrated TEM and XRD study. J. Metamorph. Geol. 18, 531–550. http://dx.doi.org/10.1046/j.1525-1314.2000.00272.x.

Arostegui, J., Sangüesa, F.J., Nieto, F., Uriarte, J.A., 2006. Thermal models and clay diagenesis in the Tertiary-Cretaceous sediments of the Alava block (Basque-Cantabrian basin, Spain). Clay Miner. 41, 791–809. http://dx.doi.org/10.1180/0009855064140219.

Bauluz, B., Peacor, D.R., Gonzalez-Lopez, J.M., 2000. Transmission electron microscopy study of illitization in pelites from the Iberian Range, Spain: Layer-by-layer replacement? Clay Clay Miner. 48, 374–384. http://dx.doi.org/10.1346/CCMN.2000.0480308.

Bauluz, B., Peacor, D.R., Ylagan, R.F., 2002. Transmission electron microscopy study of smectite illitization during hydrothermal alteration of a rhyolitic hyaloclastite from Ponza, Italy. Clay Clay Miner. 50, 157–173. http://dx.doi.org/10.1346/000986002760832766.

Beaufort, D., Baronnet, A., Lanson, B., Meunier, A., 1997. Corrensite: A single phase or a mixed-layer phyllosilicate in the saponite-to-chlorite conversion series? A case study of Sancerre-Couy deep drill hole (France). Am. Mineral. 82, 109–124.

Bettison, V., Mackinnon, J.D.R., Schiffman, P., 1991. Integrated TEM, XRD and electron microprobe investigation of mixed-layer chlorite–smectite from the Point Sal ophiolite, California. J. Metamorph. Geol. 9, 697–710 (0.1111/j.1525-1314.1991.tb00559.x).

Bourdelle, F., Parra, T., Chopin, C., Beyssac, O., 2013. A new chlorite geothermometer for diagenetic to low-grade metamorphic conditions. Contrib. Mineral. Petrol. http://dx.doi.org/10.1007/s00410-012-0832-7.

Browne, P.R.L., 1978. Hydrothermal alteration in active geothermal fields. Ann. Rev. Earth Planet. Sci. 6, 229–250.

Cathelineau, M., 1988. Cation site occupancy in chlorites and illites as a function of temperature. Clay Miner. 23, 471–485. http://dx.doi.org/10.1180/claymin.1988.023.4.13.

Cathelineau, M., Nieva, D., 1985. A chlorite solid solution geothermometer. The Los Azufres (Mexico) geothermal system. Contrib. Mineral. Petrol. 91, 235–247. http://dx.doi.org/10.1007/BF00413350.

Clavero, J., Pineda, G., Mayorga, C., Giavelli, A., Aguirre, L., Simmons, S., Martini, S., Soffia, J., Arriaza, R., Polanco, E., Achurra, L., 2011. Geological, geochemical, geophysical and first drilling data from Tinguiririca geothermal area, Central Chile. Geotherm. Res. Counc. Trans. 35, 731–734.

Cliff, G., Lorimer, G.W., 1975. The quantitative analysis of thin specimens. J. Microsc. 103, 203–207.

de Caritat, P., Hutcheon, I., Walshe, J.L., 1993. Chlorite Geothermometry - A Review. Clay Clay Miner. 41, 219–239. http://dx.doi.org/10.1346/CCMN.1993.0410210.

Dong, H., Peacor, D.R., 1996. TEM observations of coherent stacking relations in smectite, I/S and illite of shales: Evidence for MacEwan crystallites and dominance of 2M1 polytypism. Clay Clay Miner. 44, 257–275. http://dx.doi.org/10.1346/CCMN.1996.0440211.

Dong, H., Peacor, D.R., Freed, R.L., 1997. Phase relations among smectite, R1 illite–smectite, and illite. Am. Mineral. 82, 379–391.

Droguett, B., Morata, D., Clavero, J., Pineda, G., Morales, S., Carrillo, F.J., 2012. Mineralogía de alteración en el pozo Pte-1, campo geotermal Tinguiririca, Chile. Congreso Geologico Chile-2012.

Essene, E.J., Peacor, D.R., 1995. Clay mineral thermometry. A critical perspective. Clay Clay Miner. 43, 540–549. http://dx.doi.org/10.1346/CCMN.1995.0430504.

Ferrage, E., Vidal, O., Mosser-Ruck, R., Cathelinea, M., Cuadros, J., 2011. A reinvestigation of smectite illitization in experimental hydrothermal conditions: Results from X-ray diffraction and transmission electron microscopy. Am. Mineral. 96 (207–223), 1903. http://dx.doi.org/10.2138/am.2011.3945.

Fuentes, F., Aguirre, L., Vergara, M., Valdebenito, L., Fonseca, E., 2004. Miocene fossil hydrothermal system associated with a volcanic complex in the Andes of central Chile. J. Volcanol. Geotherm. Res. 138, 139–161. http://dx.doi.org/10.1016/j.jvolgeores.2004.07.001.

Giorgetti, G., Mata, P., Peacor, D.R., 2000. TEM study of the mechanism of transformation of detrital kaolinite and muscovite to illite/smectite in sediments of the Salton Sea geothermal field. Eur. J. Mineral. 12, 923–934. http://dx.doi.org/10.1127/0935-1221/2000/0012-0923.

Giorgetti, G., Mata, M.P., Peacor, D.R., 2003. Evolution of mineral assemblages and textures from sediment through hornfels in the Salton Sea geothermal field: Direct crystallization of phyllosilicates in a hydrothermal-metamorphic system. Clay Miner. 38, 113–126. http://dx.doi.org/10.1180/0009855033810082.

Grim, R.E., Güven, N., 1978. Bentonites: Geology, mineralogy, properties and uses. Elsevier, Amsterdam, The Netherlands.

Guisseau, D., Patrier-Mas, P., Beaufort, D., Girard, J.P., Inoue, A., Sanjuan, B., Petit, S., Lens, A., Genter, A., 2007. Significance of the depth-related transition montmorillonite-beidellite in the Bouillante geothermal field (Guadeloupe, Lesser Antilles). Am. Mineral. 92, 1800–1813. http://dx.doi.org/10.2138/am.2007.2398.

Guthrie, G.D., Reynolds, R.C., 1998. A coherent TEM- and XRD-description of mixed-layer illite/smectite. Can. Mineral. 36, 1421–1434.

Guthrie, G.D., Veblen, D.R., 1989a. High-resolution transmission electron microscopy of mixed-layer illite/ smectite: Computer simulations. Clay Clay Miner. 37, 1–11. http://dx.doi.org/10.1346/CCMN.1989.0370101.

Guthrie, G.D., Veblen, D.R., 1989b. High-resolution transmission electron microscopy applied to clay minerals. In: Coyne, L.M., McKeever, S.W.S., Blake, D.F. (Eds.), Spectroscopic Characterization of Minerals and their Surfaces. Symposia Series, 415. American Chemical Society, Washington, D.C.

Guthrie, G.D., Veblen, D.R., 1990. Interpreting one- dimensional high-resolution transmission electron micrographs of sheet silicates by computer simulation. Am. Mineral. 75, 276–288.

Güven, N., Grim, R., 1972. X-ray diffraction and electron optical studies on smectite and a-cristobalite associations. Clay Clay Miner. 20, 89–92.

Harvey, C.C., Browne, P.R.L., 1991. Mixed-layer clay geothermometry in the Wairakei geothermal field, New Zealand. Clay Clay Miner. 39, 614–621. http://dx.doi.org/10.1346/CCMN.1991.0390607.

Hay, R.L., Sheppard, R.A., 2001. Occurrence of zeolites in sedimentary rocks: An overview. In: Bish, D.L., Ming, D.W. (Eds.), Natural zeolites: Occurrence, properties, applications. Reviews in mineralogy and geochemistry, 45. Mineralogical Society of America, Washington, D.C, pp. 217–234.

Henley, R.W., Ellis, A.J., 1983. Geothermal systems ancient and modern: A geochemical review. Earth-Sci. Rev. 19, 1–50.

Hoffman, J., Hower, J., 1979. Clay mineral assemblages as low grade metamorphic geothermometers: Application to the thrust-faulted disturbed belt of Montana, U.S.A. In: Scholle, P.A., Schluger, P.R. (Eds.), Aspects of Diagenesis. Society Economic Palaeontologists and Mineralogist Special Publication, 26, pp. 55–79.

Inoue, A., Utada, M., 1991. Smectite-to-chloritet ransformation in thermally metamorphosedy volcanoclastic rocks in the Kamikita area, northern Honshu, Japan. Am. Mineral. 76, 628–640.

Inoue, A., Utada, M., Nagata, H., Watanabe, T., 1984. Conversion of trioctahedral smectite to interstratified chlorite/smectite in Pliocene acidic pyroclastic sediments of the Ohyu district, Akita Prefecture, Japan. Clay Sci. 6, 103–106.

Inoue, A., Meunier, A., Beaufort, D., 2004. Illite–smectite mixed-layer minerals in felsic volcaniclastic rocks from drill cores, Kakkonda, Japan. Clay Clay Miner. 52, 66–84. http://dx.doi.org/10.1346/CCMN.2004.0520108.

Inoue, A., Meunier, A., Patrier-Mas, P., Rigault, C., Beaufort, D., Vieillard, P., 2009. Application of chemical geothermometry to low-temperature trioctahedral chlorites. Clay Clay Miner. 57, 371–382. http://dx.doi.org/10.1346/CCMN.2009.0570309.

Ji, J., Browne, P.R.L., 2000. Relationship between illite crystallinity and temperature in active geothermal systems of New Zealand. Clay Clay Miner. 48, 139. http://dx.doi.org/10.1346/CCMN.2000.0480117.

Keith, T.E.C., Bargar, I.C.E., 1988. Petrology and hydrothermal mineralogy of U.S. Geological Survey Newberry 2 drill core from Newberry caldera, Oregon. J. Geophys. Res. 93, 10174–10190.

Kim, J.W., Peacor, D.R., Tessier, D., Elsass, F., 1995. A technique for maintaining texture and permanent expansion of smectite interlayers for TEM observations. Clay Clay Miner. 43, 51–57. http://dx.doi.org/10.1346/CCMN.1995.0430106.

Kogure, T., Drits, V.A., Inoue, S., 2013. Structure of mixed-layer corrensite-chlorite revealed by high-resolution transmission electron microcopy (HRTEM). Am. Mineral. 98, 1253–1260. http://dx.doi.org/10.2138/am.2013.4314. 1253.

Kristmannsdótti, H., 1976. Types of clay minerals in hydrothermally altered basaltic rocks, Reykjanes, Iceland. Jökull 26, 30–39.

Leoni, L., Lezzerini, M., Battaglia, S., Cavalcante, E., 2010. Corrensite and chlorite-rich Chl-S mixed layers in sandstones from the 'Macigno' Formation (northwestern Tuscany, Italy). Clay Miner. 45, 87–106. http://dx.doi.org/10.1180/claymin.2010.045.1.87.

Libbey, R.B., Longstaffe, F.J., Flemming, R.L., 2013. Clay mineralogy, oxygen isotope geochemistry, and water/rock ratio estimates, Te Mihi area, Wairakei geothermal field, New Zealand. Clay Clay Miner. 61, 204–217. http://dx.doi.org/10.1346/CCMN.2013.0610304.

Lindgreen, H., 1991. Elemental and structural changes in illite/smectite mixed-layer clay minerals during diagenesis in Kimmeridgian- Volgian(-Ryazanian) clays in the Central Trough, North Sea and the Norwegian-Danish Basin. Bull. Geol. Soc. Den. 39, 1–82.

Lopez-Munguira, A., Nieto, F., Morata, D., 2002. Chlorite composition and geothermometry: A comparative HRTEM/AEM-EMPA-XRD study of Cambrian basic lavas from the Ossa Morena Zone, SW Spain. Clay Miner. 37, 267–281. http://dx.doi.org/10.1180/0009855023720033.

Mas, A., Patrier, P., Beaufort, D., Genter, A., 2003. Clay-mineral signatures of fossil and active hydrothermal circulations in the geothermal system of the Lamentin Plain, Martinique. J. Volcanol. Geotherm. Res. 124, 195–218. http://dx.doi.org/10.1016/S0377-0273(03)00044-1.

Mas, A., Guisseau, D., Patrier, P., Beaufort, D., Genter, A., Sanjuan, B., Girard, J.P., 2006. Clay minerals related to the hydrothermal activity of the Bouillante geothermal field (Guadeloupe). J. Volcanol. Geotherm. Res. 158, 380–400. http://dx.doi.org/10.1016/j.jvolgeores.2006.07.010.

McDowell, S.D., Elders, W.A., 1980. Aurhigenic layer silicate minerals in borehole Elmore #1, Salton Sea geothermal field, California, USA. Contrib. Mineral. Petrol. 74, 293–310. http://dx.doi.org/10.1007/s004100050163.

Merriman, R.J., Peacor, D.R., 1999. Very low-grade metapelites; mineralogy, microfabrics and measuring reaction progress. In: Frey, M., Robinson, D. (Eds.), Low-grade metamorphism. Blackwell Sciences Ltd., Oxford, UK, pp. 10–60.

Merriman, R.J., Roberts, B., Peacor, D.R., Hirons, S.R., 1995. Strain-related differences in the crystal-growth of white mica and chlorite — A TEM and XRD study of the development of metapelitic microfabrics in the southern uplands thrust terrane, Scotland. J. Metamorph. Geol. 13, 559–576. http://dx.doi.org/10.1111/j.1525-1314.1995.tb00243.x.

Meunier, A., Velde, B., 1989. Solid solution in illite/smectite mixed layer minerals and illite. Am. Mineral. 74, 1106–1112.

Meunier, A., Inoue, A., Beaufort, D., 1991. Chemiographic analysis of trioctahedral smectite-to-chlorite conversion series from the Ohyu Caldera, Japan. Clay Clay Miner. 39, 409–415. http://dx.doi.org/10.1346/CCMN.1991.0390410.

Meunier, A., Mas, A., Beaufort, D., Patrier, P., Dudoignon, P., 2008a. Clay minerals in basalt-hawaiite rocks from Mururoa atoll (French Polynesia). I. Mineralogy. Clay Clay Miner. 56, 711–729. http://dx.doi.org/10.1346/CCMN.2008.0560611.

Meunier, A., Mas, A., Beaufort, D., Patrier, P., Dudoignon, P., 2008b. Clay minerals in basalt-hawaiite rocks from Mururoa atoll (French Polynesia). II. Petrography and geochemistry. Clay Clay Miner. 56, 730–750. http://dx.doi.org/10.1346/CCMN.2008.0560612.

Moore, D.M., Reynolds Jr., R.C., 1997. X-ray diffraction and the identification and analysis of clay minerals, 2nd ed. Oxford University Press, New York, pp. 227–296.

Morse, J.W., Casey, W.H., 1988. Ostwald processes and mineral paragenesis in sediments. Am. J. Sci. 288, 537–560.

Muffler, L.P.J., White, D.E., 1969. Active metamorphism of Upper Cenozoic sediments in the Salton Sea geothermal field and the Salton Trough, southeastern California. Geol. Soc. Am. Bull. 80, 157–182.

Nieto, F., Ortega-Huertas, M., Peacor, D.R., Aróstegui, J., 1996. Evolution of illite/smectite from early diagenesis through incipient metamorphism in sediments of the Basque-Cantabrian basin. Clay Clay Miner. 44, 304–323. http://dx.doi.org/10.1346/CCMN.1996.0440302.

Pollastro, R.M., 1993. Considerations and applications of the illite/ smectite geothermometer in hydrocarbon-bearing rocks of Miocene to Missisippian Age. Clay Clay Miner. 41, 119–133. http://dx.doi.org/10.1029/2000JB000027.

Reyes, A.G., 1990. Petrology of Philippine geothermal systems and the application of alteration mineralogy to their assessment. J. Volcanol. Geotherm. Res. 43, 279–309. http://dx.doi.org/10.1016/0377-0273(90)90057-M.

Robinson, D., Bevins, R.E., 1994. Mafic phyllosilicates in low-grade metabasites. Characterization using deconvolution analysis. Clay Miner. 29, 223–237. http://dx.doi.org/10.1180/claymin.1994.029.2.08.

Schegg, R., Leu, W., 1996. Clay mineral diagenesis and thermal history of the Thonex Well, Western Swiss Molasse Basin. Clay Clay Miner. 44, 693–705. http://dx.doi.org/10.1346/CCMN.1996.0440513.

Schiffman, P., Fridleifsson, G.O., 1991. The smectite to chlorite transition in drillhole NJ-15, Nesjavellir geothermal field, Iceland: XRD, BSE and electron microprobe investigations. J. Metamorph. Geol. 9, 679–696. http://dx.doi.org/10.1111/j.1525-1314.1991.tb00558.x.

Schiffman, P., Staudigel, H., 1995. Hydrothermal alteration of a seamount complex on La Palma, Canary Islands: implications for metamorphism in accreted terranes. Geology 22, 151–154. http://dx.doi.org/10.1130/0091-7613(1994)022<0151:HAOASC>2.3.CO;2.

Schmidt, S.Th., Robinson, D., 1997. Metamorphic grade and porosity and permeability controls on mafic phyllosilicate distributions in a regional zeolite to greenschist facies transition of the North Shore Volcanic Group, Minnesota. GSA Bull. 109, 683–697.

Shau, Y.H., Peacor, D.R., 1992. Phyllosilicates in hydrothermally altered basalts from DSDP hole 504b, leg-83 — A TEM and AEM study. Contrib. Mineral. Petrol. 112, 119–133. http://dx.doi.org/10.1007/BF00310959.

Shau, Y.H., Peacor, D.R., Essene, E.J., 1990. Corrensite and mixed-layer chlorite/smectite in metabasalt from northern Taiwan: TEM/AEM, EMPA, XRD, and optical studies. Contrib. Mineral. Petrol. 105, 123–142. http://dx.doi.org/10.1007/BF00678980.

Srodon, J., Eberl, D.D., 1984. Illite. In: Bailey, S.W. (Ed.), Micas. Reviews in mineralogy, 13. Mineralogical Society of America, Washington D.C., USA, pp. 495–544.
Uysal, I.T., Glikson, M., Golding, S.D., Audsley, F., 2000. The thermal history of the Bowen Basin, Queensland, Australia: vitrinite reflectance and the clay mineralogy of Late Permian coal measures. Tectonophysics 323, 105–129. http://dx.doi.org/10.1016/S0040-1951(00)00098-6.
Veblen, D.R., Guthrie, G.D., Livi, K.J.T., Reynolds Jr., R.C., 1990. High-resolution transmission electron microscopy and electron diffraction of mixed-layer illite/smectite: Experimental results. Clay Clay Miner. 38, 1–13. http://dx.doi.org/10.1346/CCMN.1990.0380101.
Velde, B., 1985. Clay minerals: A physico-chemical explanation of their occurrence. Elsevier, Amsterdam and New York.
Vergara, M., Levi, B., Villaroel, R., 1993. Geothermal-type alteration in a burial metamorphosed volcanic pile, central Chile. J. Metamorph. Geol. 11, 449–454. http://dx.doi.org/10.1111/j.1525-1314.1993.tb00161.x.
Vidal, O., Parra, T., Vieillard, P., 2005. Thermodynamic properties of the Tschermak solid solution in Fe-chlorite: Application to natural examples and possible role of oxidation. Am. Mineral. 90, 347–358. http://dx.doi.org/10.2138/am.2005.1554.
Vidal, O., De Andrade, V., Lewin, E., Munoz, M., Parra, T., Pascarelli, S., 2006. P-T-deformation-Fe3+/Fe2+ mapping at the thin section scale and comparison with XANES mapping: application to a garnet-bearing metapelite from the Sambagawa metamorphic belt (Japan). J. Metamorph. Geol. 24, 669–683. http://dx.doi.org/10.1111/j.1525-1314.2006.00661.x.
Warr, L.N., Nieto, F., 1998. Crystallite thickness and defect density of phyllosilicates in low-temperature metamorphic pelites: a TEM and XRD study of clay-minerals crystallinity-index standards. Can. Mineral. 36, 1453–1474.
Weaver, C.E., 1989. Clays, muds, and shales. Development in sedimentology, 44. Elsevier, New York.
Wiewióra, A., Weiss, Z., 1990. Crystallochemical classifications of phyllosilicates based on the unified system of projection of chemical composition: II The chlorite group. Clay Miner. 25, 83–92. http://dx.doi.org/10.1180/claymin.1990.025.1.09.
Yau, Y.C., Peacor, D.R., McDowell, S.D., 1987a. Smectite-to-illite reactions in Salton Sea shales: A transmission and analytical electron microscopy study. J. Sediment. Petrol. 57, 335–342.
Yau, Y.C., Peacor, D.R., Essene, E.J., 1987b. Authigenic anatase and titanite in shales from the Salton Sea geothermal field, California. Neues Jb. Mineral. Monat. 441–452.
Yau, Y.C., Peacor, D.R., Beane, R.E., Essene, E.J., McDowell, S.D., 1988. Microstructures, formation mechanism, and depth-zoning of phyllosilicates in geothermally altered shales, Salton Sea, California. Clay Clay Miner. 36, 1–10.